# Smoothing Splines in Multiscale Geopotential Determination from Satellite Data

Kerstin Hesse* and Martin Gutting†

29. April 2003

**Abstract:** *SST (satellite-to-satellite tracking)* and *SGG (satellite gravity gradiometry)* provide data that allows the determination of the first and second order radial derivative of the earth's gravitational potential on the satellite orbit, respectively. The modeling of the gravitational potential from such data is an *exponentially ill-posed problem* that demands *regularization*. In this paper, we present the numerical studies of an approach, investigated in [24] and [25], that reconstructs the potential with *spline smoothing*. In this case, spline smoothing is not just an approximation procedure but it solves the underlying compact operator equation of the SST-problem and the SGG-problem. The numerical studies in this paper are performed for a simplified geometrical scenario with simulated data, but the approach is designed to handle first or second order radial derivative data on a real satellite orbit.

**Keywords:** gravitational potential modeling, harmonic splines, harmonic wavelets, inverse problem, L-curve method, multiresolution, smoothing, smoothing parameter choice

*Author to whom correspondence should be addressed: School of Mathematics, The University of New South Wales, Sydney 2052, Australia, phone: +61 2 9385 7034, fax: +61 2 9385 7123, e-mail: kerstin@maths.unsw.edu.au

†Geomathematics Group, University of Kaiserslautern, P.O. Box 3049, 67653 Kaiserslautern, Germany, phone: +49 631 205-4826, fax: +49 631 205-4736, e-mail: gutting@mathematik.uni-kl.de, www: `http://www.mathematik.uni-kl.de/~wwwgeo`

# 1 Introduction

In this paper we present the numerical results of some investigations concerning the modeling of the earth's gravitational potential with spline smoothing from data of *satellite-to-satellite tracking (SST)* missions. In SST a low flying orbiter, like the satellite CHAMP (launched in July 2000), receives the GPS-signals of the high-flying GPS/GLONASS-satellites and measures non-gravitational accelerations with its accelerometer. Roughly speaking, the GPS-signals enable the determination of the position of the low-flying satellite with high accuracy. Knowledge of its position in turn enables it to compute (via numerical differentiation and subtraction of the non-gravitational influences with the help of the accelerometer data) the gradient of the potential along the orbit. Scalar data, which allows (from a mathematical point of view) the unique recovery of the potential, is the first order radial derivative on a closed $C^{(2)}$-regular surface at orbit altitude. Knowledge of the gradient of the potential at the orbit provides knowledge of the *first order radial derivative (scalar SST-data)* at the orbit, and that is the data our numerical simulations start with. The idea to recover the earth's gravitational potential from such scalar SST-data is formulated in [19] and is also investigated in [4], [21], and [33]. It is, of course, also possible to reconstruct the potential from vectorial data (the full gradient), but this approach is not investigated in this paper (see, for example, [19], [32]). *Satellite gravity gradiometry (SGG)* missions, like GOCE (launch planned for 2005/06), have in addition to a GPS-receiver a gradiometer on board and provide knowledge of the Hessian of the potential and consequently of its *second order radial derivative (scalar SGG-data)* along the orbit. Analogously to the SST-scenario, it is in this case possible to work with tensorial data, but this is not the objective of this publication.

Before we give a short outline of this work we want to make a few general comments concerning the problem under investigation: The determination of the earth's gravitational potential from (scalar) SST-data or SGG-data is an *exponentially ill-posed problem*, due to the ill-posedness of downward-continuation (of harmonic functions). Therefore we do not only deal with an approximation problem (i.e., the reconstruction of a function from a set of given discrete data), but we actually have to solve an *inverse problem*, which demands some means of regularization. Therefore, the problem and the methods, applied in this work, belong to approximation and regularization theory. We want to stress that the modeling of the earth's gravitational potential from data of SST and SGG missions is a research topic of paramount importance: A highly accurate model of the earth's gravitational potential helps (i) to establish a unified height system with respect to the geoid and (ii) to calculate satellite orbits and contributes to (iii) prospecting and exploration, (iv) solid earth physics, and (v) a better understanding of the geophysical system earth. Furthermore, due to the increase in measurement accuracy

and due to the unprecedented low orbit altitude of the low flying satellites in the present and future missions CHAMP, GRACE, and GOCE, data from these missions can be expected to yield potential models with an unprecedented resolution (see [9], [10], and [11]).

The focus of this paper is on the discussion of the results of the *numerical simulations* for the reconstruction of the earth's gravitational potential from SST-data and SGG-data and not on the intricacies of the theoretical mathematical approach behind. Therefore, we summarize and explain the mathematical background only briefly (with hardly any proofs) in Sections 2 and 3 and include only those results which are of special importance for our approach. The focus in this first two sections is on understanding the basic ideas of *splines* and *wavelets* in *Hilbert spaces of harmonic functions*, but not on giving an encompasssing overview of the theory behind. In Section 4 we explain our approach to the *reconstruction of the potential from SST-data and SGG-data* in detail, and in Section 5 we present the results for our *numerical studies*. We compute a smoothing spline, which is not an approximation of the measured SST-data but an approximation of the potential on and outside the earth. Spline smoothing, as applied in this problem, is *not* an approximation procedure but solves the compact ill-posed operator equation underlying the SST-problem. The resulting model is a linear combination of *strongly space-localizing* functions, which can – in contrast to outer harmonic models – capture *local features* of the potential from *only locally given data*. The numerical studies are done with simulated SST-data in a simplified geometrical situation, but we want to stress that this approach is designed to handle SST-data and SGG-data on a real satellite orbit. The theoretical background and the introduction of splines and wavelets follow the books [17] and [18]. There are, of course, other approaches to introduce wavelets on the sphere (see, for instance, [1], [2], [22], [26], [34], [35], and [36]) which could be used (by harmonic continuation) to define harmonic wavelets.

The results in this paper are part of the theses [24] and [25] to which we refer the reader for more information about the theory and for some computational aspects that are not discussed in detail here.

## 2 Notation

In this section the basic notation and the mathematical background material are briefly summarized. For more background information, the reader is referred to the books [17], [18], and [31].

Let $\mathbb{R}^N$ be the $N$-dimensional Euclidean space with the Euclidean norm $|x| := (\sum_{i=1}^N (x_i)^2)^{1/2}$ and the Euclidean inner product $x \cdot y := \sum_{i=1}^N x_i\, y_i$, where

$x = (x_1, \ldots, x_N)$, $y = (y_1, \ldots, y_N) \in \mathbb{R}^N$. The Lebesgue measure of $\mathbb{R}^N$ is denoted by $dx$.

A surface $\Sigma$ in $\mathbb{R}^3$ is called a $\mathcal{C}^{(k)}$-*regular surface*, where $2 \leq k \leq \infty$, if it satisfies the following four conditions: (i) $\Sigma$ divides $\mathbb{R}^3$ into a bounded region, denoted by $\Sigma^{\text{int}}$, the so-called *inner space of* $\Sigma$, and an unbounded region, denoted by $\Sigma^{\text{ext}}$, the so-called *outer space of* $\Sigma$, (ii) $\Sigma^{\text{int}}$ contains the origin, (iii) $\Sigma$ is closed and compact and free of double points, and (iv) $\Sigma$ is a $\mathcal{C}^{(k)}$-surface (i.e., every point $x \in \Sigma$ has an open neighborhood $\mathcal{U} \subset \mathbb{R}^3$ such that $\Sigma \cap \mathcal{U}$ has a parameterization which is $k$-times continuously differentiable).

The *sphere* $\Omega_R := \{x \in \mathbb{R}^3 \,|\, |x| = R\}$ *of radius* $R \in \mathbb{R}^+$ with center at the origin of $\mathbb{R}^3$ is a $\mathcal{C}^{(\infty)}$-regular surface and divides $\mathbb{R}^3$ into the bounded *inner space* $\Omega_R^{\text{int}}$ *(of* $\Omega_R$*)* and the unbounded *outer space* $\Omega_R^{\text{ext}}$ *(of* $\Omega_R$*)*. The *surface element of the sphere* $\Omega_R$ is denoted by $d\omega_R$, and for the unit sphere we write briefly $\Omega := \Omega_1$ and $d\omega := d\omega_1$.

If $\Sigma$ is a $\mathcal{C}^{(2)}$-regular surface and $\Omega_R$ a sphere of radius $R \in \mathbb{R}^+$ such that $\Omega_R \subset \Sigma^{\text{int}}$, then $\Omega_R$ is called a *Bjerhammar sphere for* $\Sigma$.

Throughout this work *polar coordinates* will sometimes be used: Every vector $x \in \mathbb{R}^3 \setminus \{0\}$ can be represented with respect to the canonical standard basis in $\mathbb{R}^3$ as $x = r\,\xi$, where $r = |x|$, $\xi = x/|x| \in \Omega$, and

$$\xi = (\cos(\varphi)\,\sin(\vartheta),\, \sin(\varphi)\,\sin(\vartheta),\, \cos(\vartheta))^T\,,$$

$(\varphi, \vartheta) \in [0, 2\pi) \times [0, \pi]$.

The set of all $k$-*times continuously differentiable (real valued) functions* on an open or closed set in $\mathbb{R}^N$ or a $\mathcal{C}^{(l)}$-regular surface $\mathcal{U}$ is denoted by $\mathcal{C}^{(k)}(\mathcal{U})$, $k \in \mathbb{N}_0$, and we define $\mathcal{C}^{(\infty)}(\mathcal{U}) := \bigcap_{k=0}^{\infty} \mathcal{C}^{(k)}(\mathcal{U})$, where it is understood that in case of a $\mathcal{C}^{(l)}$-regular surface only $\mathcal{C}^{(k)}(\mathcal{U})$ with $k \leq l$ can be defined. In particular, we let $\mathcal{C}(\mathcal{U}) := \mathcal{C}^{(0)}(\mathcal{U})$. The space $\mathcal{C}(\mathcal{U})$ is always endowed with the *supremum norm* $\|F\|_{\mathcal{C}(\mathcal{U})} := \sup_{x \in \mathcal{U}} |F(x)|$.

The space $\mathcal{L}^2(\mathcal{U})$ of all *Lebesgue square-integrable (real valued) functions* on a measurable set in $\mathbb{R}^N$ or a $\mathcal{C}^{(2)}$-regular surface $\mathcal{U}$ with the inner product $(F, G)_{\mathcal{L}^2(\mathcal{U})} := \int_{\mathcal{U}} F(x)\, G(x)\, dx$, $F, G \in \mathcal{L}^2(\mathcal{U})$, (where $dx$ is the Lebesgue measure and the surface element, respectively) is a Hilbert space with the induced norm $\|F\|_{\mathcal{L}^2(\mathcal{U})} := (F, F)^{1/2}_{\mathcal{L}^2(\mathcal{U})}$.

A function $F \in \mathcal{C}^{(2)}(\mathcal{U})$ on an open set $\mathcal{U} \subset \mathbb{R}^3$ is called *harmonic on* $\mathcal{U}$ if it satisfies the *Laplace equation* $\Delta F = \sum_{i=1}^3 \frac{\partial^2 F}{\partial x_i^2} = 0$ on $\mathcal{U}$, where $\Delta := \sum_{i=1}^3 \frac{\partial^2}{\partial x_i^2}$ is the *Laplace operator*. A harmonic function $F \in \mathcal{C}^{(2)}(\mathcal{U})$, defined on an unbounded

set $\mathcal{U}$, is called *regular at infinity* if it satisfies the conditions $|F(x)| = O(|x|^{-1})$ and $|\nabla F(x)| = O(|x|^{-2})$ for $|x| \to \infty$ (uniformly in all directions).

For a $\mathcal{C}^{(l)}$-regular surface $\Sigma$, where $2 \leq l \leq \infty$, we define the following *function spaces of 'potentials'*: The space $\mathrm{Pot}(\Sigma^{\mathrm{ext}})$ is the space of functions $F$ that have the following properties: (i) $F \in \mathcal{C}^{(2)}(\Sigma^{\mathrm{ext}})$, (ii) $F$ satisfies the Laplace equation $\Delta F = 0$ on $\Sigma^{\mathrm{ext}}$, and (iii) $F$ is regular at infinity. The space $\mathrm{Pot}^{(k)}(\overline{\Sigma^{\mathrm{ext}}})$, $0 \leq k \leq l$, consists of all functions $F \in \mathcal{C}^{(k)}(\overline{\Sigma^{\mathrm{ext}}})$ that satisfy in addition $F|_{\Sigma^{\mathrm{ext}}} \in \mathrm{Pot}(\Sigma^{\mathrm{ext}})$.

Let $\mathrm{Harm}_n(\Omega)$ denote the space of *spherical harmonics of degree $n$ on $\Omega$*, i.e., the space of the restrictions to $\Omega$ of all homogenous harmonic polynomials on $\mathbb{R}^3$ of degree $n$. The space $\mathrm{Harm}_n(\Omega)$ is a finite dimensional vector space with dimension $\dim(\mathrm{Harm}_n(\Omega)) = 2n+1$. Let $\{Y_{n,k}\}_{k=1,\ldots,2n+1}$ be a complete $\mathcal{L}^2(\Omega)$-orthonormal system in the space $\mathrm{Harm}_n(\Omega)$, $n \in \mathbb{N}_0$. Then $\{Y_{n,k}\}_{n\in\mathbb{N}_0;\, k=1,\ldots,2n+1}$ is a complete orthonormal system in $\mathcal{L}^2(\Omega)$ which induces a complete orthonormal system $\{Y^R_{n,k}\}_{n\in\mathbb{N}_0;\, k=1,\ldots,2n+1}$ in $\mathcal{L}^2(\Omega_R)$, via

$$Y^R_{n,k}(x) := \frac{1}{R}\, Y_{n,k}(x/|x|)\,, \qquad x \in \Omega_R\,.$$

Throughout this work, $\{Y^R_{n,k}\}_{n\in\mathbb{N}_0;\, k=1,\ldots,2n+1}$ shall always denote such a complete orthonormal system in $\mathcal{L}^2(\Omega_R)$. Every function $F \in \mathcal{L}^2(\Omega_R)$ can be expanded into a *Fourier series* with respect to the complete orthonormal system $\{Y^R_{n,k}\}_{n\in\mathbb{N}_0;\, k=1,\ldots,2n+1}$:

$$F = \sum_{n=0}^{\infty} \sum_{k=1}^{2n+1} F^R_{n,k}\, Y^R_{n,k} \tag{1}$$

with *Fourier coefficients* $\{F^R_{n,k}\}_{n\in\mathbb{N}_0;\, k=1,\ldots,2n+1}$ given by

$$F^R_{n,k} := \int_{\Omega_R} F(y)\, Y^R_{n,k}(y)\, d\omega_R(y)\,.$$

Although the span of $\{Y^R_{n,k}\}_{n\in\mathbb{N}_0;\, k=1,\ldots,2n+1}$ is dense in $\mathcal{C}(\Omega_R)$ with respect to the supremum norm, the Fourier series expansion (1) of $F \in \mathcal{L}^2(\Omega_R) \cap \mathcal{C}(\Omega_R)$ does in general not converge on $\Omega_R$ uniformly to $F$.

Let $P_n : [-1,1] \to \mathbb{R}$ denote the *Legendre polynomial of degree $n \in \mathbb{N}_0$*. The set $\{P_n\}_{n\in\mathbb{N}_0}$ of all Legendre polynomials is a complete orthogonal system in $\mathcal{L}^2([-1,1])$, and

$$\int_{-1}^{1} P_n(t)\, P_m(t)\, dt = \delta_{n,m}\, \frac{2}{(2n+1)}\,,$$

where $\delta_{n,m}$ is the Kronecker symbol: $\delta_{n,m} = 1$ if $n = m$ and $\delta_{n,m} = 0$ if $n \neq m$.

The *outer harmonics for the sphere* $\Omega_R$ (corresponding to a complete orthonormal system $\{Y_{n,k}\}_{n\in\mathbb{N}_0;\, k=1,\ldots,2n+1}$ in $\mathcal{L}^2(\Omega)$) are definded by

$$H_{n,k}(R;x) := \frac{1}{R}\left(\frac{R}{|x|}\right)^{n+1} Y_{n,k}(x/|x|)\,,$$

$x \in \mathbb{R}^3 \setminus \{0\}$; $n \in \mathbb{N}_0$; $k = 1, \ldots, 2n+1$. The function $H_{n,k}(R;x)$ is called an *outer harmonic of degree $n$ and order $k$* (for the sphere $\Omega_R$). An outer harmonic $H_{n,k}(R;\cdot)$ is in $\mathcal{C}^{(\infty)}(\mathbb{R}^3 \setminus \{0\})$, and $H_{n,k}(R;\cdot)|_{\Omega_R} = Y^R_{n,k}$. The function $H_{n,k}(R;\cdot)$ is the (uniquely determined) solution of Dirichlet's exterior boundary value problem for the Laplace equation with boundary $\Omega_R$ and boundary value $Y^R_{n,k}$ which is regular at infinity. The outer harmonics $H_{n,k}(R;\cdot)$ are elements of the space $\mathrm{Pot}^{(\infty)}(\overline{\Omega_R^{\mathrm{ext}}})$. In this work $\{H_{n,k}(R;\cdot)\}_{n\in\mathbb{N}_0;\, k=1,\ldots,2n+1}$ is always a system of outer harmonics corresponding to some complete orthonormal system $\{Y_{n,k}\}_{n\in\mathbb{N}_0;\, k=1,\ldots,2n+1}$ of spherical harmonics in $\mathcal{L}^2(\Omega)$.

The *(scalar) addition theorem for spherical harmonics* establishes a connection between the spherical harmonics of degree $n$ and the Legendre polynomial $P_n$ of degree $n$: Let $\{Y_{n,k}\}_{k=1,\ldots,2n+1}$ be an $\mathcal{L}^2(\Omega)$-orthonormal system in $\mathrm{Harm}_n(\Omega)$, $n \in \mathbb{N}_0$, then for all $\xi, \eta \in \Omega$

$$\sum_{k=1}^{2n+1} Y_{n,k}(\xi)\, Y_{n,k}(\eta) = \frac{(2n+1)}{4\pi} P_n(\xi \cdot \eta)\,.$$

This implies the *addition theorem for outer harmonics*: For $n \in \mathbb{N}_0$ and $x, y \in \overline{\Omega_R^{\mathrm{ext}}}$

$$\sum_{k=1}^{2n+1} H_{n,k}(R;x)\, H_{n,k}(R;y) = \frac{(2n+1)}{4\pi\, R^2} \left(\frac{R^2}{|x|\,|y|}\right)^{n+1} P_n\left(\frac{x}{|x|} \cdot \frac{y}{|y|}\right).$$

# 3 Splines and Wavelets in Hilbert Spaces of Harmonic Functions

In this section the relevant definitions and theorems from the theory of splines and wavelets in Hilbert spaces of harmonic functions are briefly recapitulated. For more details the reader is reader is referred to, for example, [17] and [18]. The type of splines, introduced in Subsection 3.2, is the key ingredient in the approach and goes back to the publications [5], [13], [14], [15], and [16].

## 3.1 Hilbert Spaces of Harmonic Functions

We begin with the introduction of certain classes of Hilbert spaces in which we will define splines and wavelets later on. The sequence $\{A_n\}_{n\in\mathbb{N}_0} \subset \mathbb{R}^+$ in the next definition allows much flexibility in the choice of the Hilbert space and will be chosen later to satisfy our particular needs. The assumption $A_n \geq C$ for all $n \in \mathbb{N}_0$ with some $C > 0$ simply guarantees that the functions in the Hilbert space, restricted to $\Omega_R$, are in $\mathcal{L}^2(\Omega_R)$.

**Definition 3.1** *Let $\{A_n\}_{n\in\mathbb{N}_0} \subset \mathbb{R}^+$ satisfy the condition $A_n \geq C$ for all $n \in \mathbb{N}_0$ with some constant $C \in \mathbb{R}^+$. For $F \in \operatorname{span}\{H_{n,k}(R;\cdot) \,|\, n \in \mathbb{N}_0\,;\, k = 1,\dots,2n+1\}$, we can compute the Fourier coefficients*

$$F_{n,k}^R := \int_{\Omega_R} F(y)\, Y_{n,k}^R(y)\, d\omega_R(y)\,,$$

*$n \in \mathbb{N}_0\,;\, k+1,\dots,2n+1$, and we define*

$$\|F\|_{\mathcal{H}} := \left( \sum_{n=0}^{\infty} \sum_{k=1}^{2n+1} A_n^2\, (F_{n,k}^R)^2 \right)^{1/2}.$$

*The space $\mathcal{H} = \mathcal{H}(\{A_n\}; \overline{\Omega_R^{\text{ext}}})$, defined by*

$$\mathcal{H} := \overline{\operatorname{span}\{H_{n,k}(R;\cdot) \,|\, n \in \mathbb{N}_0\,;\, k = 1,\dots,2n+1\}}^{\|\cdot\|_{\mathcal{H}}},$$

*with the inner product*

$$(F,G)_{\mathcal{H}} := \sum_{n=0}^{\infty} \sum_{k=1}^{2n+1} A_n^2\, F_{n,k}^R\, G_{n,k}^R$$

*for $F, G \in \mathcal{H}$, is a* (Sobolev-like) Hilbert space.

We denote the inner product of $F \in \mathcal{H}$ and $G \in \mathcal{H}$ also by

$$F *_{\mathcal{H}} G := (F,G)_{\mathcal{H}}$$

and call it the *convolution of $F$ and $G$*. A function $F \in \mathcal{H}$ can be (formally) represented by its *series expansion in terms of outer harmonics*

$$F = \sum_{n=0}^{\infty} \sum_{k=1}^{2n+1} F_{n,k}^R\, H_{n,k}(R;\cdot)\,, \tag{2}$$

and this function $F$ and its series expansion (2) have the following properties:

- the series expansion (2) of $F \in \mathcal{H}$ is, restricted to $\Omega_R$, convergent in $\mathcal{L}^2(\Omega_R)$-sense,
- the series expansion (2) of $F \in \mathcal{H}$ is, restricted to $\overline{\Omega_r^{\text{ext}}}$ with $r > R$, uniformly convergent, and $F|_{\Omega_R^{\text{ext}}}$ is continuous,
- the series expansion (2) of $F \in \mathcal{H}$ may be differentiated term by term in $x \in \Omega_R^{\text{ext}}$ (for partial derivatives of arbitrary order), and the differentiated series is uniformly convergent to the respective derivative of $F$ on every $\overline{\Omega_r^{\text{ext}}}$ with $r > R$,
- $F \in \mathcal{H}$ is harmonic on $\Omega_R^{\text{ext}}$ and regular at infinity.

If, in addition, the sequence $\{A_n\}_{n\in\mathbb{N}_0}$ satisfies the so-called *summability condition*

$$\sum_{n=0}^{\infty} \frac{(2n+1)}{A_n^2} < \infty \tag{3}$$

then $\mathcal{H}$ is a *reproducing kernel Hilbert space* with the *reproducing kernel*

$$\begin{aligned} K_{\mathcal{H}}(x,y) &:= \sum_{n=0}^{\infty} \sum_{k=1}^{2n+1} \frac{1}{A_n^2} H_{n,k}(R;x)\, H_{n,k}(R;y) \\ &= \sum_{n=0}^{\infty} \frac{(2n+1)}{4\pi R^2 A_n^2} \left(\frac{R^2}{|x|\,|y|}\right)^{n+1} P_n\left(\frac{x\cdot y}{|x|\,|y|}\right), \end{aligned}$$

$x, y \in \overline{\Omega_R^{\text{ext}}}$. This means that $K_{\mathcal{H}}(x,\cdot) \in \mathcal{H}$ for all (fixed) $x \in \overline{\Omega_R^{\text{ext}}}$ and that $K_{\mathcal{H}}$ satisfies the *reproducing property*

$$(F, K_{\mathcal{H}}(x,\cdot))_{\mathcal{H}} = F(x)$$

for all $x \in \overline{\Omega_R^{\text{ext}}}$ and for all $F \in \mathcal{H}$. It should be noted that the reproducing kernel $K_{\mathcal{H}}$ depends only on $|x|$, $|y|$, and $(x\cdot y)/(|x|\,|y|)$. A separable Hilbert space $\mathcal{H}$ is a reproducing kernel Hilbert space if and only if all evaluation functionals $\mathcal{L}_x : \mathcal{H} \to \mathbb{R}$, $G \mapsto \mathcal{L}_x G := G(x)$, $x \in \overline{\Omega_R^{\text{ext}}}$, are continuous. If $\mathcal{H}$, defined as in Definition 3.1, is a reproducing kernel Hilbert space all functions in $\mathcal{H}$ are continuous, i.e., $\mathcal{H} \subset \mathcal{C}(\overline{\Omega_R^{\text{ext}}})$, and their series expansions (2) converge uniformly on $\overline{\Omega_R^{\text{ext}}}$. For more information about reproducing kernel Hilbert spaces the reader is referred to [3].

Next, we give some relevant examples of Hilbert spaces $\mathcal{H}$, defined as in Definition 3.1.

**Example 3.2** *The norm of $\mathcal{H} = \mathcal{H}(\{1\}; \overline{\Omega_R^{\text{ext}}})$ is the $\mathcal{L}^2(\Omega_R)$-norm, i.e.,*

$$\|F\|_{\mathcal{H}} = \left(\int_{\Omega_R} |F(x)|^2\, d\omega_R(x)\right)^{1/2}.$$

**Example 3.3** *Let $h \in (0,1)$. Then the space $\mathcal{H} = \mathcal{H}(\{h^{-n/2}\}; \overline{\Omega_R^{\text{ext}}})$ is a reproducing kernel Hilbert space with the reproducing kernel*

$$K_{\mathcal{H}}(x,y) = \frac{1}{4\pi} \frac{|x|^2|y|^2 - h^2R^4}{(|x|^2|y|^2 + h^2R^4 - 2\,h\,R^2(x\cdot y))^{3/2}}.$$

**Example 3.4** *Let $h \in (0,1)$. Then the space $\mathcal{H} = \mathcal{H}(\{(n+\frac{1}{2})^{1/2}\, h^{-n/2}\}; \overline{\Omega_R^{\text{ext}}})$ is a reproducing kernel Hilbert space with the reproducing kernel*

$$K_{\mathcal{H}}(x,y) = \frac{1}{2\pi} \frac{1}{(|x|^2|y|^2 + h^2R^4 - 2\,h\,R^2(x\cdot y))^{1/2}}.$$

The representations of the reproducing kernels of the spaces in Examples 3.3 and 3.4 as elementary functions follow easily from the relations

$$\begin{aligned} \frac{1}{(1+\gamma^2-2\,\gamma\,t)^{1/2}} &= \sum_{n=0}^{\infty} \gamma^n\, P_n(t)\,, \\ \frac{1-\gamma^2}{(1+\gamma^2-2\,\gamma\,t)^{3/2}} &= \sum_{n=0}^{\infty} (2n+1)\,\gamma^n\, P_n(t) \end{aligned}$$

for all $t \in [-1,1]$ and all $\gamma \in (-1,1)$ which can, for example, be found in [18].

Figure 1 shows the reproducing kernel of the space in Example 3.3, restricted to the sphere $\Omega_R$, for various parameters $h$ as a function of $t := (x \cdot y)/|x|\,|y|$, where $t$ is parameterized by $t = \cos(\theta)$, $\theta \in [-\pi, \pi]$.

The reproducing kernels $K_{\mathcal{H}}$ for the classes of spaces in Examples 3.3 and 3.4 are *space-localizing*: The closer $h$ gets to one, the stronger is the space-localization of the reproducing kernel.

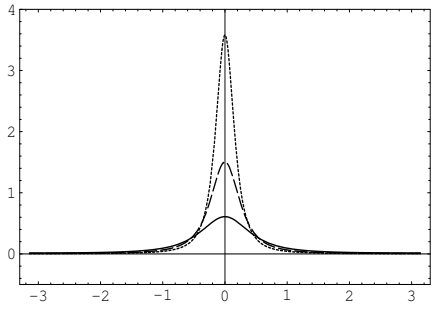


**Figure 1:** *The reproducing kernel $K_{\mathcal{H}}$ of $\mathcal{H} = \mathcal{H}(\{h^{-n/2}\}; \overline{\Omega_R^{\text{ext}}})$, restricted to the sphere $\Omega_R$, where $R = 1$ and $|x| = 1$, $x$ fixed, and $h = 0.55$ (solid), $h = 0.7$ (dashed), $h = 0.8$ (dotted).*

## 3.2 Harmonic Splines

Next, we introduce splines in the Hilbert spaces $\mathcal{H}$. These splines have to be seen more in analogy to radial basis functions than in analogy to cubic polynomial splines (though it should be noted that they are *not* radial basis functions). Roughly speaking, in our applications a spline space is spanned by strongly space-localizing functions which are related to the set of measurements.

**Definition 3.5** *Let $\mathcal{H}$ be a Hilbert space as defined in Definition 3.1, and let $\mathcal{L}_1, \ldots, \mathcal{L}_N$ be $N$ bounded linear functionals on $\mathcal{H}$. Denote by $L_i$ the represen-*

*ter of* $\mathcal{L}_i$, $i \in \{1, \ldots, N\}$, *i.e.,* $\mathcal{L}_i F = (F, L_i)_{\mathcal{H}} = F *_{\mathcal{H}} L_i$ *for all* $F \in \mathcal{H}$. *Then any function of the form*

$$S := \sum_{i=1}^{N} \alpha_i \, L_i$$

*with the coefficient vector* $\alpha := (\alpha_1, \ldots, \alpha_N)^T \in \mathbb{R}^N$ *is called a* spline (relative to $\mathcal{L}_1, \ldots, \mathcal{L}_N$). *The space of all splines relative to* $\mathcal{L}_1, \ldots, \mathcal{L}_N$ *is denoted by*

$$\mathcal{S}_{\mathcal{H}}(\mathcal{L}_1, \ldots, \mathcal{L}_N) := \operatorname{span} \{ L_i \mid i = 1, \ldots, N \} \, .$$

The next lemma follows immediately from Definition 3.5.

**Lemma 3.6** *Let the notation and the assumptions be as in Definition 3.5. Then for any spline* $S = \sum_{i=1}^{N} \alpha_i \, L_i$ *in* $\mathcal{S}_{\mathcal{H}}(\mathcal{L}_1, \ldots, \mathcal{L}_N)$

$$(F, S)_{\mathcal{H}} = F *_{\mathcal{H}} S = \sum_{i=1}^{N} \alpha_i \, \mathcal{L}_i F \qquad \text{for all } F \in \mathcal{H} \, .$$

The most simple example is the representer of an evaluation functional $\mathcal{L}_x : \mathcal{H} \to \mathbb{R}$, $\mathcal{L}_x F := F(x)$, $x \in \overline{\Omega_R^{\text{ext}}}$ fixed, in a reproducing kernel Hilbert space $\mathcal{H}$ with reproducing kernel $K_{\mathcal{H}}$: the representer is given by $L_x := K_{\mathcal{H}}(x, \cdot)$.

Next, we formulate the *spline interpolation problem*: Let $\mathcal{H}$ be a Hilbert space, defined as in Definition 3.1, and let $\mathcal{L}_1, \ldots, \mathcal{L}_N$ be $N$ bounded linear functionals on $\mathcal{H}$ with representers $L_1, \ldots, L_N$. We define the *set of interpolating functions of a function* $F \in \mathcal{H}$ *relative to* $\mathcal{L}_1, \ldots, \mathcal{L}_N$ by

$$\mathcal{I}^F_{\mathcal{L}_1, \ldots, \mathcal{L}_N} := \{ G \in \mathcal{H} \mid \mathcal{L}_i G = \mathcal{L}_i F \text{ for } i = 1, \ldots, N \} \, .$$

The *spline interpolation problem (relative to* $\mathcal{L}_1, \ldots, \mathcal{L}_N$*)* is to find an interpolating spline $S$, i.e., $S \in \mathcal{S}_{\mathcal{H}}(\mathcal{L}_1, \ldots, \mathcal{L}_N) \cap \mathcal{I}^F_{\mathcal{L}_1, \ldots, \mathcal{L}_N}$.

**Theorem 3.7** *Let* $\mathcal{H}$ *be defined as in Definition 3.1, and let* $\mathcal{L}_1, \ldots, \mathcal{L}_N$ *be* $N$ *bounded linear functionals on* $\mathcal{H}$ *with representers* $L_1, \ldots, L_N$. *Let* $F \in \mathcal{H}$ *be given. There is* one and only one *interpolating spline* $S^F = \sum_{i=1}^{N} \alpha_i \, L_i$ *of* $F$ *in* $\mathcal{S}_{\mathcal{H}}(\mathcal{L}_1, \ldots, \mathcal{L}_N) \cap \mathcal{I}^F_{\mathcal{L}_1, \ldots, \mathcal{L}_N}$. *This spline is the* orthogonal projection of $F$ onto the spline space $\mathcal{S}_{\mathcal{H}}(\mathcal{L}_1, \ldots, \mathcal{L}_N)$. *It satisfies the following minimum property:*

$$\|S - G\|^2_{\mathcal{H}} = \|S^F - G\|^2_{\mathcal{H}} + \|S - S^F\|^2_{\mathcal{H}}$$

*for all* $S \in \mathcal{S}_{\mathcal{H}}(\mathcal{L}_1, \ldots, \mathcal{L}_N)$ *and all* $G \in \mathcal{I}^F_{\mathcal{L}_1, \ldots, \mathcal{L}_N}$. *In particular,* $S = 0$ *shows that the interpolating spline* $S^F$ *of* $F$ *is the interpolating function in* $\mathcal{H}$ *with minimum*

*norm. The coefficient vector* $\alpha = (\alpha_1, \ldots, \alpha_N)^T$ *of the interpolating spline* $S^F$ *is the solution of the linear system of equations*

$$\sum_{i=1}^{N} \alpha_i \, (L_i, L_k)_{\mathcal{H}} = \mathcal{L}_k F \,, \qquad k = 1, \ldots, N \,.$$

In practice, the values $\mathcal{L}_1 F, \ldots, \mathcal{L}_N F$ will not be known exactly but only be given approximately in the form of noisy measurements, i.e., we know $\mathcal{L}_i F + \epsilon_i$, $i = 1, \ldots, N$, where $\epsilon_1, \ldots, \epsilon_N$ represent the measurement errors. In this case, one has to perform *spline smoothing* instead of spline interpolation.

**Theorem 3.8** *Let* $\mathcal{H}$ *be a Hilbert space as defined in Definition 3.1, and let* $\mathcal{L}_1, \ldots, \mathcal{L}_N$ *be* $N$ *bounded linear functionals on* $\mathcal{H}$ *with the representers* $L_1, \ldots, L_N$. *Suppose* $b = (b_1, \ldots, b_N)^T \in \mathbb{R}^N$ *is an arbitrarily given vector and* $\lambda \in \mathbb{R}^+$ *a positive real parameter. Then there exists one and only one spline* $S_\lambda = \sum_{i=1}^N \alpha_i^\lambda \, L_i$ *in* $\mathcal{S}_{\mathcal{H}}(\mathcal{L}_1, \ldots, \mathcal{L}_N)$ *that minimizes the linear functional*

$$\mu_\lambda(\alpha) := \sum_{i=1}^{N} (\mathcal{L}_i S - b_i)^2 + \lambda \, \|S\|_{\mathcal{H}}^2 \,, \tag{4}$$

*where* $S = \sum_{i=1}^N \alpha_i \, L_i$ *with the coefficient vector* $\alpha = (\alpha_1, \ldots, \alpha_N)^T$. *The coefficient vector* $\alpha^\lambda = (\alpha_1^\lambda, \ldots, \alpha_N^\lambda)^T$ *of this minimizing spline* $S_\lambda$ *is the uniquely determined solution of the linear system of equations*

$$\sum_{i=1}^{N} \alpha_i \, (L_i, L_k)_{\mathcal{H}} + \lambda \, \alpha_k = b_k \,, \quad k = 1, \ldots, N. \tag{5}$$

The proofs of Theorems 3.7 and 3.8 can, for example, be found in [17].

Usually the vector $b$ in Theorem 3.8 will be a vector of noisy measurements $b = (\mathcal{L}_1 F + \epsilon_1, \ldots, \mathcal{L}_N F + \epsilon_N)^T$. The most important question concerning Theorem 3.8 is the choice of the *smoothing parameter* $\lambda$. For $\lambda = 0$ we would get the interpolating spline, assuming that (5) is still solvable. The larger $\lambda > 0$ gets, the less weight is put on data fitting and the more weight is put on the smoothness of the solution (in the sense that the norm of the solution is small). Clearly, the smoothing parameter $\lambda$ has to be chosen depending on the measurement errors. We remark that spline smoothing as introduced in Theorem 3.8 is done in the usual way, as it is, for example, introduced in [37].

In order to derive *smoothing parameter choice rules*, we write the functional (4) and the linear system of equations (5) in a different way: Using the notation

$\mathbf{A} := [(L_i, L_k)_{\mathcal{H}}]_{i,k=1,\dots,N}$, $\mathbf{Id} := [\delta_{i,k}]_{i,k=1,\dots,N}$, we see after some easy computations that

$$\begin{aligned} (4) \quad &\Leftrightarrow \quad \mu_\lambda(\alpha) = |\mathbf{A}\,\alpha - b|^2 + \lambda\,\alpha^T \mathbf{A}\,\alpha\,, \\ (5) \quad &\Leftrightarrow \quad (\mathbf{A} + \lambda\,\mathbf{Id})\,\alpha = b\,, \end{aligned} \tag{6}$$

where $|\cdot|$ is the Euclidean norm in $\mathbb{R}^N$. The matrix $\mathbf{A}$ is symmetric. If we assume that $\mathcal{L}_1, \dots, \mathcal{L}_N$ are linearly independent then $\mathbf{A}$ is even invertible and positive definite, and we can define the $\mathbf{A}$-norm $\|x\|_{\mathbf{A}} := (x^T \mathbf{A}\,x)^{1/2}$ on $\mathbb{R}^N$, and (6) is equivalent to

$$\mu_\lambda(\alpha) = |\mathbf{A}\,\alpha - b|^2 + \lambda\,\|\alpha\|_{\mathbf{A}}^2\,. \tag{7}$$

Functional (7) has a strong similarity to the *Tikhonov functional*, where our smoothing parameter $\lambda$ corresponds to the regularization parameter in Tikhonov regularization. Applying some methods which are used to derive parameter choice strategies for Tikhonov regularization, we obtain smoothing parameter choice rules. For more information on Tikhonov regularization see, for example, [8], [27]. The adaptation of two such strategies, namely the *L-curve method* and *Morozov's discrepancy principle* to spline smoothing is discussed in [25] in more detail. In the studies in this paper the L-curve method is used, and we sketch briefly how it works.

In the *L-curve method*, we plot the two terms in the functional (4) depending on $\lambda$ (for the minimizing splines $S_\lambda$) in a double-logarithmic parametric plot:

$$\lambda \mapsto \left( \ln \left( \left( \sum_{i=1}^{N} (\mathcal{L}_i S_\lambda - b_i)^2 \right)^{1/2} \right), \ln \left( \|S_\lambda\|_{\mathcal{H}} \right) \right). \tag{8}$$

This demands the computation of smoothing splines $S_\lambda$ for a certain range of smoothing parameters $\lambda$. The resulting curve should be L-shaped, and the L-curve criterion predicts that a suitable smoothing parameter lies in the corner point of the L. The L-curve method is an empirical method, and it lacks a sound mathematical foundation, but, for practical purposes, it has the advantage that it is numerically not too expensive and that it does not demand any knowledge about the measurement errors. It should be noted that there are scenarios in which the L-curve method failed, but it seems to be working satisfactory for the smoothing parameter choice in spline smoothing. For more information about the L-curve method, the reader is referred to [8] and the references therein.

Finally, we give a few examples of bounded linear functionals and their representers, namely *first* and *second order radial derivatives* in points $x$ in the outer space $\Omega_R^{\text{ext}}$, because these describe SST-data and SGG-data. A proof that first and second order radial derivatives in points $x \in \Omega_R^{\text{ext}}$ are bounded linear functionals on $\mathcal{H}$, defined as in Definition 3.1, can be found in [25]. Due to the fact that the spaces $\mathcal{H}$ in Examples 3.3 and 3.4 are reproducing kernel Hilbert spaces, the representers

in these spaces can be easily obtained by applying the bounded linear functional to the reproducing kernel $K_{\mathcal{H}}$, i.e., the representer of $\mathcal{L} : \mathcal{H} \to \mathbb{R}$, $F \mapsto \mathcal{L}F := \frac{\partial^\kappa F(x)}{\partial r^\kappa}$, with $\kappa \in \{1, 2\}$ and $x \in \Omega_R^{\text{ext}}$, is given by

$$L(y) := \frac{\partial^\kappa K_{\mathcal{H}}(y, x)}{\partial r_x^\kappa}, \qquad y \in \overline{\Omega_R^{\text{ext}}},$$

where the index $x$ at the radius $r$ indicates that we take the derivative with respect to the second variable $x$.

**Example 3.9** *Let $\mathcal{H} = \mathcal{H}(\{h^{-n/2}\}; \overline{\Omega_R^{\text{ext}}})$ with $h \in (0, 1)$. The* first order radial derivative $\mathcal{L} : \mathcal{H} \to \mathbb{R}$, $F \mapsto \mathcal{L}F := \frac{\partial F(x)}{\partial r}$, in the point $x \in \Omega_R^{\text{ext}}$ *has the representer $L \in \mathcal{H}$, given by*

$$\begin{aligned} L(y) \quad := \quad & \frac{-|y| \left(3\, h^3 R^6\, (x \cdot y)(|x|\,|y|)^{-1} + |x|^3 |y|^3\right)}{4\pi\, \left(h^2 R^4 - 2\, h\, R^2 (x \cdot y) + |x|^2\, |y|^2\right)^{5/2}} \\ & - \frac{|y| \left(-5\, h^2 R^4 |x|\,|y| + h\, R^2\, |x|\,|y| (x \cdot y)\right)}{4\pi\, \left(h^2 R^4 - 2\, h\, R^2 (x \cdot y) + |x|^2\, |y|^2\right)^{5/2}}. \end{aligned}$$

**Example 3.10** *Let $\mathcal{H} = \mathcal{H}(\{h^{-n/2}\}; \overline{\Omega_R^{\text{ext}}})$ with $h \in (0, 1)$. The* second order radial derivative $\mathcal{L} : \mathcal{H} \to \mathbb{R}$, $F \mapsto \mathcal{L}F := \frac{\partial^2 F(x)}{\partial r^2}$, in the point $x \in \Omega_R^{\text{ext}}$ *has the representer $L \in \mathcal{H}$, given by*

$$\begin{aligned} L(y) \quad := \quad & \frac{|y|^2 \left(5\, h^4 R^8 \left(1 - 3 (x \cdot y)^2 (|x|\,|y|)^{-2}\right) + 4\, h\, R^2 |x|^2 |y|^2 (x \cdot y)\right)}{4\pi\, (h^2 R^4 - 2\, h\, R^2 (x \cdot y) + |x|^2\, |y|^2)^{7/2}} \\ & + \frac{|y|^2 \left(2\, |x|^4\, |y|^4 - h^2\, R^4 \left(23\, |x|^2\, |y|^2 + (x \cdot y)^2\right) + 28\, h^3 R^6 (x \cdot y)\right)}{4\pi\, (h^2 R^4 - 2\, h\, R^2 (x \cdot y) + |x|^2\, |y|^2)^{7/2}}. \end{aligned}$$

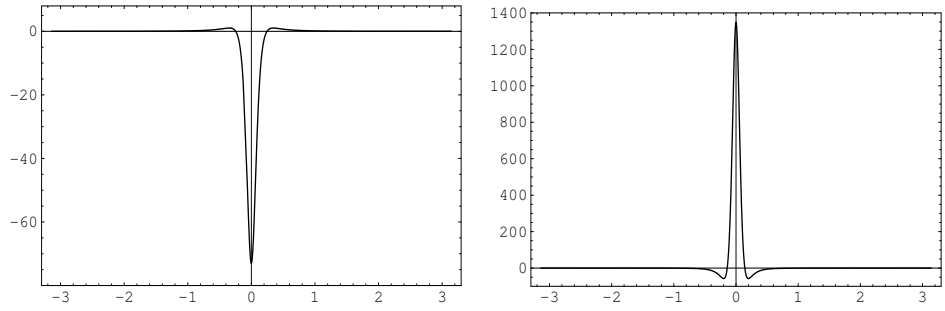


**Figure 2:** *The representer of a first (left picture) and a second order radial derivative (right picture) on $\mathcal{H} = \mathcal{H}(\{h^{-n/2}\}; \overline{\Omega_R^{\text{ext}}})$, restricted to the sphere $\Omega_R$, for $R = 1$, $h = 0.9$, $|x| = 1.06$, $x$ fixed (see Examples 3.9 and 3.10).*

For the spaces in Example 3.4 we can also obtain elementary representations of the representers of first and second order radial derivatives, and the pictures of the representers look similar to the ones in Figure 2 (see [24], [25]). The representers of first and second order radial derivatives in the classes of spaces in Examples 3.3 and 3.4 are strongly *space-localizing* functions. As with the reproducing kernel itself, the space-localization of the representers depends on the parameter $h$: the closer $h$ is to one, the stronger is the space-localization. For practical purposes, this means that an interpolating or smoothing spline with respect to evaluation functionals or first or second order radial derivatives (in points of a finite grid in $\Omega_R^{\text{ext}}$) can only be expected to yield a sensible approximation if the areas where the representers are not small overlap sufficiently. Due to the space-localizing nature of the representers, it is also possible to compute a spline which is a *local approximation* of a function from *only locally given data*. In this case, Gibbs' phenomena will occur at the boundary of the local region, where the data are given.

## 3.3 Harmonic Scaling Functions and Wavelets

Harmonic scaling functions and wavelets are defined similarly as introduced in [17]. A scaling function is a family of kernels $\{\Phi_j\}_{j\in\mathbb{N}_0}$, which 'approximate the Dirac' in the sense that the convolution $x \mapsto F *_{\mathcal{H}} \Phi_j(x,\cdot)$ of a function $F \in \mathcal{H}$ with these kernels gets a better and better approximation of $F$ as $j$ increases. Wavelets help to describe the difference between two such subsequent approximations of $F$.

**Definition 3.11** *Let $\mathcal{H} = \mathcal{H}(\{A_n\}; \overline{\Omega_R^{\text{ext}}})$ be defined as in Definition 3.1, and let $\{\Phi_j\}_{j\in\mathbb{N}_0}$ be a sequence of kernels*

$$\Phi_j(x,y) := \sum_{n=0}^{\infty} \sum_{k=1}^{2n+1} \frac{(\Phi_j)^\wedge(n)}{A_n^2} H_{n,k}(R;x)\, H_{n,k}(R;y)\,, \tag{9}$$

*$x, y \in \overline{\Omega_R^{\text{ext}}}$, where the sequences $\{(\Phi_j)^\wedge(n)\}_{n\in\mathbb{N}_0}$, $j \in \mathbb{N}_0$, of real numbers have to satisfy*

$$\lim_{n\to\infty} (\Phi_j)^\wedge(n) = 0 \tag{10}$$

*and*

$$\sum_{n=0}^{\infty} \frac{(2n+1)}{A_n^2} \left|(\Phi_j)^\wedge(n)\right| < \infty\,. \tag{11}$$

*The sequence $\{\Phi_j\}_{j\in\mathbb{N}_0}$ is called a* (harmonic) scaling function for $\mathcal{H}$ *if for all $F \in \mathcal{H}$*

$$\lim_{j\to\infty} F *_{\mathcal{H}} \Phi_j(x,\cdot) = F(x)\,, \qquad x \in \overline{\Omega_R^{\text{ext}}}\,, \tag{12}$$

*in $\|\cdot\|_{\mathcal{H}}$-sense. The family $\{\{(\Phi_j)^\wedge(n)\}_{n\in\mathbb{N}_0}\}_{j\in\mathbb{N}_0}$ is called the* generating symbol *of the scaling function $\{\Phi_j\}_{j\in\mathbb{N}_0}$.*

Conditions (10) and (11) guarantee that $\Phi_j(x,\cdot) \in \mathcal{H}$ for any fixed $x \in \overline{\Omega_R^{\mathrm{ext}}}$, that the convolution in (12) is well-defined, and that $\Phi_j$ is a continuous kernel. It should be noted that condition (10) could have been replaced by two slightly weaker conditions, but we rather demand (10) because it seems to be a natural property of a scaling function. Computation of the convolution in (12) yields

$$F *_{\mathcal{H}} \Phi_j(x,\cdot) = \sum_{n=0}^{\infty} \sum_{k=1}^{2n+1} (\Phi_j)^\wedge(n)\, F_{n,k}^R\, H_{n,k}(R;x)\,,$$

$x \in \overline{\Omega_R^{\mathrm{ext}}}$, which implies that $\lim_{j\to\infty}(\Phi_j)^\wedge(n) = 1$ has to be satisfied for all $n \in \mathbb{N}_0$.

**Lemma 3.12** *Let $\mathcal{H} = \mathcal{H}(\{A_n\}; \overline{\Omega_R^{\mathrm{ext}}})$ be defined as in Definition 3.1, and assume that $\{\Phi_j\}_{j\in\mathbb{N}_0}$ is a sequence of kernels of the form (9) which satisfies (10), (11), and the conditions*

*(i) there exists a constant $C > 0$ such that $|(\Phi_j)^\wedge(n)| \le C$ for all $n \in \mathbb{N}_0$ and all $j \in \mathbb{N}_0$,*

*(ii) $\lim_{j\to\infty}(\Phi_j)^\wedge(n) = 1$ for all $n \in \mathbb{N}_0$.*

*Then $\{\Phi_j\}_{j\in\mathbb{N}_0}$ is a scaling function for $\mathcal{H}$.*

For a better understanding, we give a sketch of the proof: The error $\|F - F *_{\mathcal{H}} \Phi_j\|_{\mathcal{H}}$ reads

$$\|F - F *_{\mathcal{H}} \Phi_j\|_{\mathcal{H}} = \left( \sum_{n=0}^{\infty} \sum_{k=1}^{2n+1} A_n^2\, (F_{n,k}^R)^2\, \left(1 - (\Phi_j)^\wedge(n)\right)^2 \right)^{1/2}. \tag{13}$$

Condition (i) implies that $|1 - (\Phi_j)^\wedge(n)| \le 1 + C$ uniformly in $n \in \mathbb{N}_0$ and $j \in \mathbb{N}_0$, so that we are allowed to interchange the limit for $j \to \infty$ and the summation in equation (13).

**Definition 3.13** *Let $\{\Phi_j\}_{j\in\mathbb{N}_0}$ be a scaling function for $\mathcal{H} = \mathcal{H}(\{A_n\}; \overline{\Omega_R^{\mathrm{ext}}})$ with the generating symbol $\{\{(\Phi_j)^\wedge(n)\}_{n\in\mathbb{N}_0}\}_{j\in\mathbb{N}_0}$. The sequence of kernels $\{\Psi_j\}_{j\in\mathbb{N}_0}$, defined by*

$$\Psi_j(x,y) := \sum_{n=0}^{\infty} \sum_{k=1}^{2n+1} \frac{(\Psi_j)^\wedge(n)}{A_n^2}\, H_{n,k}(R;x)\, H_{n,k}(R;y)\,,$$

*$x, y \in \overline{\Omega_R^{\mathrm{ext}}}$, where the sequences $\{(\Psi_j)^\wedge(n)\}_{n\in\mathbb{N}_0}$, $j \in \mathbb{N}_0$, are given by*

$$(\Psi_j)^\wedge(n) := (\Phi_{j+1})^\wedge(n) - (\Phi_j)^\wedge(n)\,,$$

*is called the* (harmonic) wavelet corresponding to the scaling function $\{\Phi_j\}_{j\in\mathbb{N}_0}$. *The family $\{\{(\Psi_j)^\wedge(n)\}_{n\in\mathbb{N}_0}\}_{j\in\mathbb{N}_0}$ is called the generating symbol of $\{\Psi_j\}_{j\in\mathbb{N}_0}$.*

The definition of the wavelet $\{\Psi_j\}_{j\in\mathbb{N}_0}$ implies that

$$\begin{aligned} \Psi_j &= \Phi_{j+1} - \Phi_j\,, \qquad j \in \mathbb{N}_0\,, \\ \Phi_{J+1} &= \Phi_{J_0} + \sum_{j=J_0}^{J} \Psi_j\,, \qquad J, J_0 \in \mathbb{N}_0\,,\ J \geq J_0\,. \end{aligned} \tag{14}$$

This leads to the *decomposition and reconstruction theorem.*

**Theorem 3.14** *Let $\{\Phi_j\}_{j\in\mathbb{N}_0}$ be a scaling function for $\mathcal{H} = \mathcal{H}(\{A_n\}; \overline{\Omega_R^{\text{ext}}})$ with the corresponding wavelet $\{\Psi_j\}_{j\in\mathbb{N}_0}$. Define the sequences $\{P_j\}_{j\in\mathbb{N}_0}$ and $\{T_j\}_{j\in\mathbb{N}_0}$ of bounded linear operators on $\mathcal{H}$, by*

$$\begin{aligned} P_j &: \mathcal{H} \to \mathcal{H}\,, \qquad P_j F(x) := F *_{\mathcal{H}} \Phi_j(x,\cdot)\,, \\ T_j &: \mathcal{H} \to \mathcal{H}\,, \qquad T_j F(x) := F *_{\mathcal{H}} \Psi_j(x,\cdot)\,. \end{aligned}$$

*Then*

$$P_{J+1} = P_{J_0} + \sum_{j=J_0}^{J} T_j\,, \qquad J, J_0 \in \mathbb{N}_0\,,\ J \geq J_0\,,$$

*and any $F \in \mathcal{H}$ can be reconstructed in $\mathcal{H}$ by*

$$F = P_{J_0} F + \lim_{J\to\infty} \sum_{j=J_0}^{J} T_j F\,. \tag{15}$$

Theorem 3.14 is a direct consequence of (14) and the definition of a scaling function.

The idea behind (15) in the last theorem is that $P_{J_0}F$ is a *low-pass filtered* basic approximation of the function $F$. By adding successively the $T_jF$, $j = J_0, \ldots, J$, we add more and more *details* (*band-pass filtered* versions) of $F$ to improve this approximation. This allows it to reconstruct the function $F$ with different resolutions and also to see how it changes from one approximation to the next.

Lastly, we give some examples of scaling functions and wavelets. The most simple example is the bandlimited Shannon scaling function and the corresponding wavelet. *Bandlimited* means that the series expansions of almost all the kernels (9) are finite sums or, in other words, that for almost all $j \in \mathbb{N}_0$ only finitely many members of the sequence $\{(\Phi_j)^\wedge(n)\}_{n\in\mathbb{N}_0}$ are different from zero. A scaling function that is not bandlimited is called *non-bandlimited.*

**Example 3.15** *Let $\{\gamma_j\}_{j\in\mathbb{N}_0} \subset (0,1]$ be a strict monotonically decreasing sequence with $\lim_{j\to\infty}\gamma_j = 0$. Then the generating symbol $\{\{(\Phi_j)^\wedge(n)\}_{n\in\mathbb{N}_0}\}_{j\in\mathbb{N}_0}$ of the* Shannon scaling function *$\{\Phi_j\}_{j\in\mathbb{N}_0}$ for the space $\mathcal{H} = \mathcal{H}(\{A_n\}; \overline{\Omega_R^{\text{ext}}})$ is defined by*

$$(\Phi_j)^\wedge(n) := \begin{cases} 1 & \text{if} \quad 0 \leq n < \gamma_j^{-1} \\ 0 & \text{if} \quad \gamma_j^{-1} \leq n < \infty\,. \end{cases}$$

*Hence, the* Shannon scaling function $\{\Phi_j\}_{j\in\mathbb{N}_0}$ *for* $\mathcal{H} = \mathcal{H}(\{A_n\};\overline{\Omega_R^{\mathrm{ext}}})$ *is given by*

$$\Phi_j(x,y) = \sum_{n<\gamma_j^{-1}} \frac{(2n+1)}{4\pi R^2 A_n^2} \left(\frac{R^2}{|x|\,|y|}\right)^{n+1} P_n\left(\frac{x\cdot y}{|x|\,|y|}\right).$$

Unfortunately, the Shannon scaling function and its wavelet oscillate rather strongly. The next examples are non-bandlimited scaling functions.

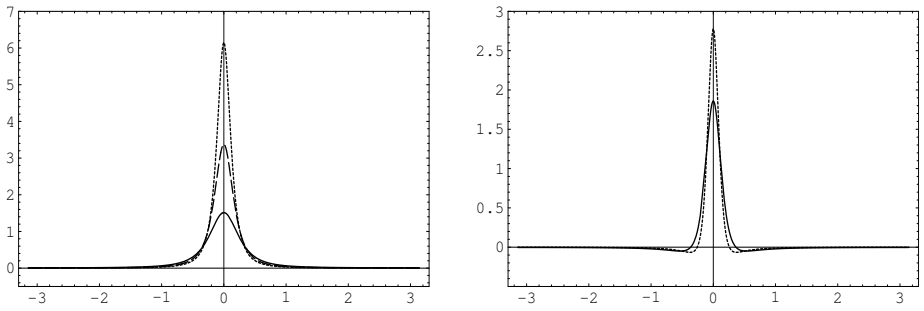


**Figure 3:** *Kernels* $\Phi_j$ *of the Abel-Poisson scaling function (left picture) for* $\mathcal{H} = \mathcal{H}(\{h^{-n/2}\};\overline{\Omega_R^{\mathrm{ext}}})$ *(Example 3.16 (a)) for* $j = 2$ *(solid),* $j = 3$ *(dashed),* $j = 4$ *(dotted), and the kernels* $\Psi_j$ *of the corresponding Abel-Poisson wavelet (right picture) for* $j = 2$ *(solid),* $j = 3$ *(dotted), where* $\gamma_j = 2^{-j}$, $\alpha = 1$, $y \in \Omega_R$, $x$ *fixed,* $|x| = R$, $R = 1$, *and* $h = 0.9$.

**Example 3.16** *Let* $\{\gamma_j\}_{j\in\mathbb{N}_0} \subset \mathbb{R}^+$ *be a strict monotonically decreasing sequence of positive real numbers with* $\lim_{j\to\infty}\gamma_j = 0$, *and define* $Q : [0,\infty) \to [0,\infty)$, $Q(t) := \alpha\, t$, *where* $\alpha \in \mathbb{R}^+$. *The generating symbol* $\{\{(\Phi_j)^\wedge(n)\}_{n\in\mathbb{N}_0}\}_{j\in\mathbb{N}_0}$ *of the* (exponential) Abel-Poisson scaling function $\{\Phi_j\}_{j\in\mathbb{N}_0}$ *for* $\mathcal{H} = \mathcal{H}(\{A_n\};\overline{\Omega_R^{\mathrm{ext}}})$ *is defined by*

$$(\Phi_j)^\wedge(n) := e^{-\gamma_j Q(n)} = e^{-\gamma_j \alpha n},$$

*and the corresponding* (exponential) Abel-Poisson wavelet $\{\Psi_j\}_{j\in\mathbb{N}_0}$ *has the generating symbol* $\{\{(\Psi_j)^\wedge(n)\}_{n\in\mathbb{N}_0}\}_{j\in\mathbb{N}_0}$ *given by*

$$(\Psi_j)^\wedge(n) := e^{-\gamma_{j+1} Q(n)} - e^{-\gamma_j Q(n)}.$$

*For the following classes of spaces, the kernels* $\Phi_j$ *of the* Abel-Poisson scaling function $\{\Phi_j\}_{j\in\mathbb{N}_0}$ *are available as elementary functions:*

*(a) Let* $h \in (0,1)$. *Then the Abel-Poisson scaling function* $\{\Phi_j\}_{j\in\mathbb{N}_0}$ *for the Hilbert space* $\mathcal{H}(\{h^{-n/2}\};\overline{\Omega_R^{\mathrm{ext}}})$ *is given by*

$$\Phi_j(x,y) = \frac{1}{4\pi} \frac{|x|^2|y|^2 - h^2R^4 e^{-2\gamma_j\alpha}}{\left(|x|^2|y|^2 + h^2R^4\, e^{-2\gamma_j\alpha} - 2\,h\,R^2 e^{-\gamma_j\alpha}(x\cdot y)\right)^{3/2}}.$$

*(b) Let $h \in (0,1)$. Then the Abel-Poisson scaling function $\{\Phi_j\}_{j\in\mathbb{N}_0}$ for the Hilbert space $\mathcal{H}(\{(n+\frac{1}{2})^{1/2}\, h^{-n/2}\}; \overline{\Omega_R^{\text{ext}}})$ is given by*

$$\Phi_j(x,y) = \frac{1}{2\pi} \frac{1}{\left(|x|^2|y|^2 + h^2R^4e^{-2\gamma_j\alpha} - 2\,h\,R^2e^{-\gamma_j\alpha}(x\cdot y)\right)^{1/2}}\,.$$

# 4 Reconstruction of the Gravitational Potential from SST-Data or SGG-Data

In this section the approximation of the potential with a smoothing spline, computed from given noisy SST-data or SGG-data, is explained. It should be noted that spline smoothing and spline interpolation, as defined in Subsection 3.2, are not only means of approximation in the sense that they allow us to reconstruct an observable from given data. They even enable the solution of integral equations, in our case the SST-problem and the SGG-problem. The numerical results for the described approach will be presented in Section 5.

## 4.1 Formulation of the SST-Problem and the SGG-Problem

Let the *earth's surface* $\Sigma_{\text{E}}$ be a $\mathcal{C}^{(2)}$-regular surface, and choose a Bjerhammar sphere $\Omega_R$ for $\Sigma_{\text{E}}$ (usually close below $\Sigma_{\text{E}}$, see Figure 4). We assume that the *earth's gravitational potential* $V$ is in $\text{Pot}^{(0)}(\overline{\Sigma_{\text{E}}^{\text{ext}}})$ and that we are given *noisy SST-data* ($\kappa = 1$) or *noisy SGG-data* ($\kappa = 2$)

$$\left\{ \left( x_i, \frac{\partial^\kappa V(x_i)}{\partial r^\kappa} + \epsilon_i \right) \,\middle|\, i = 1,\ldots,N \right\} \tag{16}$$

on a pointset $X_N = \{x_1,\ldots,x_N\}$ on the satellite orbit. The values $\epsilon_1,\ldots,\epsilon_N \in \mathbb{R}$ are the measurement errors. As the given data (16) is satellite data, we may assume that

$$\sup_{x\in\Sigma_{\text{E}}} |x| < \min_{i=1,\ldots,N} |x_i|\,.$$

The task (*SST-problem* and *SGG-problem*) is to reconstruct the earth's gravitational potential on and outside the earth's surface $\Sigma_{\text{E}}$ with the help of the given SST-data and SGG-data (16), respectively. This is clearly an *ill-posed problem*, due to the *ill-posedness of downward-continuation*.

We remark that it is also possible to model, instead of the earth's gravitational potential $V$, the potential $V - W$, where $W \in \text{Pot}^{(0)}(\overline{\Sigma_{\text{E}}^{\text{ext}}})$ is a known *model which captures the global trends* of the earth's gravitational potential. Such a model $W$ could, for example, be an outer harmonic model which includes only outer harmonic

contributions of a low degree. To start with *'residual data'* of $V - W$ is also a very sensible approach because the spline method, investigated here, works with space-localizing functions and is particularly suited for the description of the *finer local structures* of the gravitational potential.

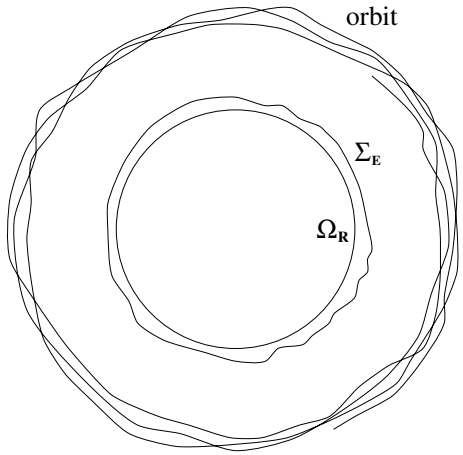


**Figure 4:** $\Sigma_{\mathrm{E}}$ *is the earth's surface, and* $\Omega_R$ *is a Bjerhammar sphere for* $\Sigma_{\mathrm{E}}$.

## 4.2 Solution of the SST-Problem and the SGG-Problem

A motivation of our approach is given by the following theorem which follows from the Runge-Walsh approximation theorem (see [12]) and an extension of Helly's theorem (see [39]). For a proof of Theorem 4.1 see [25].

**Theorem 4.1** *Let* $\Sigma$ *be a* $\mathcal{C}^{(2)}$*-regular surface and let* $\Omega_R$ *be a Bjerhammar sphere for* $\Sigma$. *Assume that* $X_N = \{x_1, \ldots, x_N\} \subset \Sigma^{\mathrm{ext}}$ *is a pointset in* $\Sigma^{\mathrm{ext}}$ *such that* $\sup_{x\in\Sigma} |x| < \min_{i=1,\ldots,N} |x_i|$. *Let* $G \in \mathrm{Pot}^{(0)}(\overline{\Sigma^{\mathrm{ext}}})$. *Given* $\varepsilon > 0$, *there exists a function* $F \in \mathcal{H} = \mathcal{H}(\{A_n\}; \overline{\Omega_R^{\mathrm{ext}}})$ *such that*

$$\sup_{x\in\overline{\Sigma^{\mathrm{ext}}}} |G(x) - F(x)| \leq \varepsilon$$

*and*

$$\frac{\partial^\kappa F(x_i)}{\partial r^\kappa} = \frac{\partial^\kappa G(x_i)}{\partial r^\kappa} \qquad \text{for } i = 1, \ldots, N\,,$$

*where* $\kappa \in \{1, 2\}$.

Application of Theorem 4.1 to the SST-problem and the SGG-problem, respectively, yields that, given $\varepsilon > 0$, in a space $\mathcal{H} = \mathcal{H}(\{A_n\}; \overline{\Omega_R^{\text{ext}}})$ there exists a function $U \in \mathcal{H}$ such that

$$\sup_{x \in \overline{\Sigma_{\text{E}}^{\text{ext}}}} |V(x) - U(x)| \leq \varepsilon$$

and

$$\frac{\partial^\kappa U(x_i)}{\partial r^\kappa} = \frac{\partial^\kappa V(x_i)}{\partial r^\kappa} \qquad \text{for } i = 1, \ldots, N\,.$$

This function $U$ can now be approximated by a smoothing spline $S_\lambda$ in $\mathcal{H}$ computed from the data (16) of $V$, where the smoothing parameter $\lambda$ has to be chosen depending on the errors $\epsilon_1, \ldots, \epsilon_N$. If the SST-data and SGG-data, respectively, is 'dense enough' and has sufficient accuracy, this smoothing spline can be expected to be a good approximation of $U$, and consequently $V$, at the satellite orbit. As the SST-problem and the SGG-problem are *exponentially ill-posed problems*, it seems (from the theoretical point of view) not predictable whether spline smoothing yields sufficient regularization to guarantee that $S_\lambda$ is also a good approximation of $U$ and $V$ with respect to $\|\cdot\|_{\mathcal{C}(\overline{\Sigma_{\text{E}}^{\text{ext}}})}$. Our numerical experiments, however, have shown that the smoothing spline $S_\lambda$ is a good approximation of the potential $V$ everywhere on $\overline{\Sigma_{\text{E}}^{\text{ext}}}$. If this were not the case, we could compensate the 'remaining ill-posedness' by convolving the spline $S_\lambda$ with a suitable scaling function. For a more detailed discussion of these points the reader is referred to [25].

The computation of the smoothing spline $S_\lambda = \sum_{i=1}^N \alpha_i^\lambda L_i$ from the given data (16) demands the solution of the following linear system:

$$\sum_{i=1}^{N} \alpha_i \, (L_i, L_l)_{\mathcal{H}} + \lambda \, \alpha_l = \frac{\partial^\kappa V(x_l)}{\partial r^\kappa} + \epsilon_l \,, \qquad l = 1, \ldots, N\,, \tag{17}$$

where the bounded linear functionals $\mathcal{L}_1, \ldots, \mathcal{L}_N$ on the Hilbert space $\mathcal{H}$ with the representers $L_1, \ldots, L_N$ are given by

$$\mathcal{L}_i : \mathcal{H} \to \mathbb{R}, \qquad F \mapsto \mathcal{L}_i F := \frac{\partial^\kappa F(x_i)}{\partial r^\kappa}\,.$$

In case $N$ is large (i.e., $N > 10{,}000$), this becomes a time-consuming task. In order to save time and memory, (17) can be solved efficiently with a domain decomposition method, *the Schwarz alternating algorithm*. We have implemented a multiplicative variant of this algorithm, which splits the large matrix in (17) in a number of smaller submatrices of the same type and solves smaller systems, corresponding to these submatrices, subsequently in each iterative step. This multiplicative variant has still the 'standard structure' of an iterative algorithm and can be used for the solution of any linear system with a *positive definite symmetric matrix*. As the main focus of this publication is on the presentation of the numerical

results, we do not discuss here the solution of the linear systems in detail, but give only a pseudocode of the algorithm in Section 5 and refer the reader to [6], [20], [24], and [25], where the multiplicative variant of the Schwarz alternating algorithm and its application to the computation of (harmonic) splines are discussed in great detail. For more general information about the Schwarz alternating algorithm we refer to, for instance, [7], [23], [29], [30], [38].

Concerning the smoothing spline $S_\lambda$, it should be noted that the given data are values of the first or second order radial derivative of the potential at the satellite orbit, whereas the computed spline $S_\lambda$ is *not* an approximation of this data but an *approximation of the potential on* $\overline{\Sigma_{\mathrm{E}}^{\mathrm{ext}}}$. This means that the computation of the spline actually solves the SST-problem and the SGG-problem, respectively: the spline is not an approximation of the given data but a solution of the ill-posed SST-problem or SGG-problem, both of which can be formulated as compact pseudodifferential operator equations (see, for example, [17] or [25]).

Finally, we discuss the important question of the *choice of the Hilbert space* $\mathcal{H} = \mathcal{H}(\{A_n\}; \overline{\Omega_R^{\mathrm{ext}}})$. The spaces discussed in Examples 3.3 and 3.4 are reproducing kernel Hilbert spaces with strongly space-localizing reproducing kernels $K_{\mathcal{H}}$, and the representers $L_i := \frac{\partial^\kappa}{\partial r_{x_i}^\kappa} K_{\mathcal{H}}(\cdot, x_i)$ of the bounded linear functionals $\mathcal{L}_i : \mathcal{H} \to \mathbb{R}$, $\mathcal{L}_i F := \frac{\partial^\kappa F(x_i)}{\partial r^\kappa}$, $i = 1, \ldots, N$, are also strongly space-localizing. It is clear that the areas where these functions are not small have to overlap sufficiently; otherwise the computed spline will be a 'collection of peaks' at the measurement points. On the other hand, the stronger the space-localization of the representers $L_i$, $i = 1, \ldots, N$, the better is the condition of the matrix. We have to balance these two contrary demands. Clearly, the right amount of space-localization depends on the density of the pointset. For the classes of spaces given in Examples 3.3 and 3.4, we can tune the space localization with the parameter $h$. Furthermore, the space $\mathcal{H}$ should be chosen such that the representers $L_i$ and the matrix entries in the linear system (17) have representations as elementary functions, because this will simplify the numerical computations. This is satisfied for the spaces $\mathcal{H}$ in Examples 3.3 and 3.4. (If the $L_i$ and the matrix entries are not available as elementary functions then we have to truncate their series expansions, which causes numerical errors. Furthermore, the computation of the truncated series expansion is rather time-consuming.)

# 5 Numerical Results

In Subsection 5.1, we describe the setup for our numerical simulations for an SST scenario, and in Subsections 5.2 and 5.3 we present and discuss the numerical results.

## 5.1 Recovery of the Potential from SST-Data

For the numerical simulations of the reconstruction of the earth's gravitational potential from noisy SST-data, we use the *NASA model EGM96* (Earth Gravitational Model 96, see [28] and `http://cddisa.gfsc.nasa.gov/926/egm96.html`), which provides a model of the earth's gravitational potential in form of a set of (real fully normalized) spherical harmonic coefficients $\{V_{n,k}^R\}_{n=0,\dots,360;\,-n\le k\le n}$ related to a sphere $\Omega_R$, whose radius $R = 6378136.3$ m coincides with the equatorial radius of the earth, and to the $\mathcal{L}^2(\Omega)$-orthonormal system of fully normalized spherical harmonics $\{Y_{n,k}\}_{n\in\mathbb{N}_0;\,-n\le k\le n}$, commonly used in geosciences. The corresponding outer harmonics for the sphere $\Omega_R$ are denoted by $\{H_{n,k}(R;\cdot)\}_{n\in\mathbb{N}_0;\,-n\le k\le n}$, and we regard outer harmonic contributions to EGM96 from degrees $n \in \{5,\dots,80\}$, i.e., the *test gravitational potential* used for our simulation is

$$\widetilde{V}(x) = \Gamma\, M \sum_{n=5}^{80} \sum_{k=-n}^{n} V_{n,k}^R\, H_{n,k}(R;x)\,, \qquad x \in \overline{\Omega_R^{\rm ext}}\,,$$

where $\Gamma\, M = 3986004.415 \cdot 10^8$ m$^3$ s$^{-2}$ is the product of the gravitational constant $\Gamma$ and the mass of the earth $M$. The *SST-signal* is then given by the function

$$\frac{\partial \widetilde{V}(x)}{\partial r} = \Gamma M \sum_{n=5}^{80} \sum_{k=-n}^{n} \frac{-(n+1)}{|x|}\, V_{n,k}^R\, H_{n,k}(R;x)\,, \qquad x \in \Omega_R^{\rm ext}\,. \tag{18}$$

The simulated SST-data are generated on an *ellipsoid of revolution* $E_{\rm S}$ (with semiminor axis $b_1 = 6825674.24$ m and the semimajor axis $b_2 = 6853093.49$ m) whose rotational axis is the semiminor axis pointing in the direction of the North Pole. The center of the ellipsoid $E_{\rm S}$ is the origin of the Euclidean space $\mathbb{R}^3$ (see Figure 6). The *simulated noisy SST-data*

$$\left\{ \left( x_i, \frac{\partial \widetilde{V}(x_i)}{\partial r} + \epsilon_i \right) \,\middle|\, i = 1,\dots,N \right\} \tag{19}$$

are generated in the points of a *Reuter grid* (or a local subset of a Reuter grid) with grid parameter $\tau$, which are projected from the sphere $\Omega_R$ along the radial direction onto the ellipsoid of revolution $E_{\rm S}$.

**Definition 5.1** *For $\tau \in \mathbb{N}$ the* Reuter grid $X_N = \{(r, \varphi_{i,j}, \vartheta_i)\}$ *on $\Omega_r$ is defined as follows:*

*(a)* $\vartheta_0 := 0$, $\varphi_{0,1} := 0$ *(North Pole),*

*(b)* $\Delta\vartheta = \pi/\tau$,

*(c)* $\vartheta_i := i\,\Delta\vartheta$, $1 \le i \le \tau - 1$,

*(d)* $\tau_i := \left\lfloor 2\pi \left( \arccos\left( \frac{\cos(\Delta\vartheta) - \cos^2(\vartheta_i)}{\sin^2(\vartheta_i)} \right) \right)^{-1} \right\rfloor$,

*(e)* $\varphi_{i,j} := (j - \frac{1}{2})(2\pi/\tau_i)$, $1 \le j \le \tau_i$,

*(f)* $\vartheta_\tau := \pi$, $\varphi_{\tau,1} := 0$ *(South Pole),*

*where* $\lfloor x \rfloor := \sup\{n \in \mathbb{Z} \mid n \le x\}$. *The number of points* $N = N(\tau)$ *in the Reuter grid depends on the* grid parameter $\tau$ *and can be estimated by* $N(\tau) \le 2 + \frac{4}{\pi}\tau^2$.

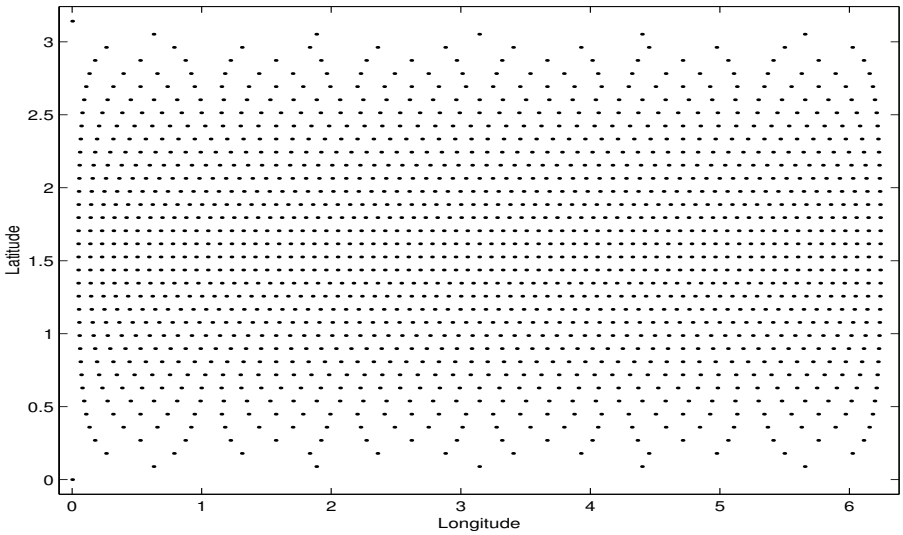


**Figure 5:** *Reuter grid with grid parameter* $\tau = 35$ *and* $N = 1542$ *points.*

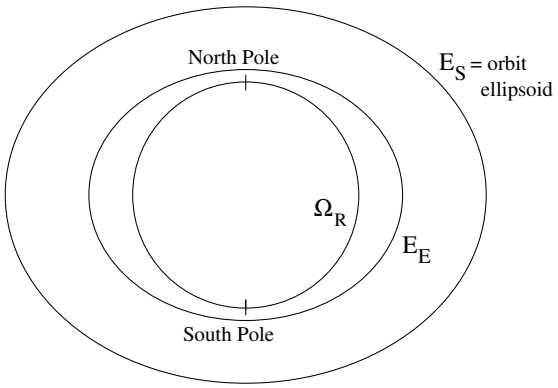


**Figure 6:** *The geometrical situation in the numerical study.*

The noise $\epsilon_1, \ldots, \epsilon_N$ is generated with a random number generator which is based on the standard Gauss normal distribution with a *noise level of* 2% of the the mean absolute value of the SST-signal in the domain where the SST-data are given. We compute a smoothing spline $S_\lambda = \sum_{i=1}^N \alpha_i^\lambda L_i$ in the reproducing kernel Hilbert space $\mathcal{H} = \mathcal{H}(\{h^{-n/2}\}; \overline{\Omega_R^{\text{ext}}})$ from the given data (19), i.e., the smoothing spline $S_\lambda$ is in $\mathcal{S}_\mathcal{H}(\mathcal{L}_1, \ldots, \mathcal{L}_N)$, where $\mathcal{L}_i : \mathcal{H} \to \mathbb{R}$ is defined by $\mathcal{L}_i F := \frac{\partial F(x_i)}{\partial r}$ and has the representer $L_i$, given in Example 3.9. If we denote the reproducing kernel of $\mathcal{H}$ by $K_\mathcal{H} : \overline{\Omega_R^{\text{ext}}} \times \overline{\Omega_R^{\text{ext}}} \to \mathbb{R}$ the linear system (17) for the determination of the coefficient vector of the smoothing spline $S_\lambda$ takes the form

$$\sum_{i=1}^N \alpha_i \frac{\partial}{\partial r_{x_k}} \frac{\partial}{\partial r_{x_i}} K_\mathcal{H}(x_k, x_i) + \lambda \alpha_k = \frac{\partial \widetilde{V}(x_k)}{\partial r} + \epsilon_k \,, \qquad k = 1, \ldots, N \,. \tag{20}$$

The entries of its matrix are available as elementary functions because the reproducing kernel $K_\mathcal{H}$ has a representation as an elementary function (see Example 3.3). The linear system (20) is solved with the following *multiplicative variant of the Schwarz alternating algorithm*:

Let $X_{N_1}, \ldots, X_{N_M}$, where $X_{N_r} := \{x_1^r, \ldots, x_{N_r}^r\}$, $r \in \{1, \ldots, M\}$, be $M$ possibly overlapping subsets of the measurement pointset $X_N = \{x_1, \ldots, x_N\} \subset E_{\text{S}}$ such that

$$\bigcup_{r=1}^M X_{N_r} = X_N \,.$$

For $r \in \{1, \ldots, M\}$, we define the *restriction operator* $R_r : \mathbb{R}^N \to \mathbb{R}^{N_r}$, $w \mapsto R_r(w)$, $R_r(w) = ((R_r(w))_1, \ldots, (R_r(w))_{N_r})^T$, by

$$(R_r(w))_i := w_j \qquad \text{for the index } j \in \{1, \ldots, N\} \text{ with } x_i^r = x_j \,,$$

and the *embedding operator* $I_r : \mathbb{R}^{N_r} \to \mathbb{R}^N$, $z \mapsto I_r(z) = ((I_r(z))_1, \ldots, (I_r(z))_N)^T$, by

$$(I_r(z))_i := \begin{cases} z_j & \text{if there exists } j \in \{1, \ldots, N_r\} \text{ with } x_i = x_j^r \\ 0 & \text{else.} \end{cases}$$

Then the multiplicative variant of the Schwarz alternating algorithm for the solution of the spline smoothing problem (20) in the space $\mathcal{H} = \mathcal{H}(\{h^{-n/2}\}; \overline{\Omega_R^{\text{ext}}})$ with the smoothing parameter $\lambda \in \mathbb{R}^+$ reads as follows:

**Algorithm 5.2**
*define for* $r = 1, \ldots, M$ *the matrices* $\mathbf{A}_r := \left[\frac{\partial}{\partial r_{x_i^r}} \frac{\partial}{\partial r_{x_j^r}} K_\mathcal{H}(x_j^r, x_i^r) + \lambda \delta_{i,j}\right]_{i,j=1,\ldots,N_r}$
*set* $f_0 := \left(\frac{\partial \widetilde{V}(x_1)}{\partial r} + \epsilon_1, \ldots, \frac{\partial \widetilde{V}(x_N)}{\partial r} + \epsilon_N\right)^T$ *and* $a_0 := (0, \ldots, 0)^T \in \mathbb{R}^N$
*for* $n = 0, 1, 2, \ldots$ *do*
  *for* $r = 1, \ldots, M$ *do*

*solve* $\mathbf{A}_r\, b = R_r(f_{nM+(r-1)})$, *where* $b = (b_1, \ldots, b_{N_r})^T \in \mathbb{R}^{N_r}$
*update* $a_{nM+r} := a_{nM+(r-1)} + I_r(b)$
*update* $f_{nM+r} := f_{nM+(r-1)} - \lambda\, I_r(b) - \left( \left( \sum_{i=1}^{N_r} b_i \frac{\partial^2 K_{\mathcal{H}}(x_k, x_i^r)}{\partial r_{x_i^r} \partial r_{x_k}} \right)_{k=1,\ldots,N} \right)^T$
*until* $\frac{|f_{(n+1)M}|}{|f_0|} \leq \varepsilon$
*compute* $S^G := \sum_{i=1}^{N} (a_{(n+1)M})_i \frac{\partial}{\partial r_{x_i}} K_{\mathcal{H}}(\cdot, x_i)$

The subdivision of the sphere (or a subset of the sphere, which is a rectangle in the $(\varphi, \vartheta)$-plane) is based one a subdivision of the $(\varphi, \vartheta)$-plane in (overlapping) rectangles which are of the same surface area on the sphere. In our implementation of Algorithm 5.2, the QR factorization of the matrices $\mathbf{A}_r$ of the subproblems is computed in advance in a preprocessing step (with the FORTRAN software package LAPACK) and is kept in memory, so that the subproblems can be efficiently solved with the associated LAPACK QR backward substitution routine in the iterative steps of the algorithm. The accuracy tolerance $\varepsilon$ in the stopping criterion of Algorithm 5.2 is chosen, for all computations as either $\varepsilon := 10^{-10}$ or $\varepsilon := 10^{-8}$. The implementation was done in C++, using the Prama 2001 C++ library of M. Fengler. For the details the reader is referred to [24] and [25]. After the smoothing spline $S_\lambda$ with the smoothing parameter $\lambda$ has been calculated with the multiplicative Schwarz alternating algorithm from the noisy SST-data (19), it is evaluated on a $(\varphi, \vartheta)$-grid $\{y_1, \ldots, y_{L^2}\}$ of $L \times L$ points (equiangular in $\varphi$ and equiangular in $\vartheta$, i.e., the angles of the grid points are all of the form $\varphi = \varphi_0 + k\,\Delta\varphi$, $\vartheta = \vartheta_0 + k\,\Delta\vartheta$, where $0 \leq k \leq (L-1)$, $k \in \mathbb{N}_0$, but in general $\Delta\varphi \neq \Delta\vartheta$) on the *ellipsoid of revolution* $E_{\mathrm{E}}$ with semiminor axis $a_1 = 6384520.82$ m and semimajor axis $a_2 = 6405998.92$ m. The semiminor axis of $E_{\mathrm{E}}$ is parallel to the semiminor axis of $E_{\mathrm{S}}$, and the ellipsoid $E_{\mathrm{E}}$ rotates around its semiminor axis and has its center in the origin of $\mathbb{R}^3$ (see Figure 6). The *mean absolute error* (mean error) and the *rooted mean square error* (rms error) of the smoothing spline $S_\lambda$,

$$\text{mean error} := \frac{1}{L^2} \sum_{i=1}^{L^2} |\widetilde{V}(y_i) - S_\lambda(y_i)|\,,$$

$$\text{rms error} := \left( \frac{1}{L^2} \sum_{i=1}^{L^2} |\widetilde{V}(y_i) - S_\lambda(y_i)|^2 \right)^{1/2},$$

as a model for the gravitational potential $\widetilde{V}$ on $E_{\mathrm{E}}$ are computed. For a suitably chosen smoothing parameter $\lambda$, the smoothing spline $S_\lambda$ shows sufficient accuracy as an approximation of $\widetilde{V}$, and no further smoothing (via convolution with a scaling function) is required.

A reconstruction of the potential $\widetilde{V}$ in form of a *multiresolution* is derived by convolving the smoothing spline $S_\lambda$ with the kernels of the Abel-Poisson scaling

function $\{\Phi_j\}_{j\in\mathbb{N}_0}$ for $\mathcal{H}$, with generating symbol $\{\{(\Phi_j)^\wedge(n)\}_{n\in\mathbb{N}_0}\}_{j\in\mathbb{N}_0}$, defined by $(\Phi_j)^\wedge(n) := e^{-2^{-j}n}$ (i.e., $\alpha = 1$ and $\gamma_j = 2^{-j}$ in Example 3.16), and of the corresponding wavelet $\{\Psi_j\}_{j\in\mathbb{N}_0}$. The resolution of the model $S_\lambda = \sum_{i=1}^N \alpha_i^\lambda L_i$ of $\widetilde{V}$ at scale $j \in \mathbb{N}_0$ is then given by

$$\begin{aligned} P_j S_\lambda(x) &= S_\lambda *_{\mathcal{H}(\{h^{-n/2}\};\overline{\Omega_R^{\mathrm{ext}}})} \Phi_j(x,\cdot) \\ &= \sum_{i=1}^N \alpha_i^\lambda \frac{\partial}{\partial r_{x_i}} \Phi_j(x,x_i)\,, \qquad x \in \overline{\Sigma_{\mathrm{E}}^{\mathrm{ext}}}\,, \end{aligned} \tag{21}$$

where $\frac{\partial}{\partial r_{x_i}}\Phi_j(x,x_i)$ can be easily computed as an elementary function, due to the elementary representation of $\Phi_j$. The detail $T_j S_\lambda$ of the model $S_\lambda$ at scale $j$ is given by

$$\begin{aligned} T_j S_\lambda(x) &= S_\lambda *_{\mathcal{H}(\{h^{-n/2}\};\overline{\Omega_R^{\mathrm{ext}}})} \Psi_j(x,\cdot) \\ &= P_{j+1} S_\lambda(x) - P_j S_\lambda(x)\,, \qquad x \in \overline{\Sigma_{\mathrm{E}}^{\mathrm{ext}}}\,. \end{aligned} \tag{22}$$

Clearly, $P_j S_\lambda$ and $T_j S_\lambda$ can be easily evaluated, due to the representations of $\Phi_j$ and $\Psi_j$ as elementary functions.

In this study, the sphere $\Omega_R$ as well as the two ellipsoids of revolution $E_{\mathrm{E}}$ and $E_{\mathrm{S}}$ are parameterized in polar coordinates $(r,\varphi,\vartheta)$ with $(\varphi,\vartheta) \in [0,2\pi)\times[0,\pi]$, and a local domain on any of these surfaces will be described by specification of the restrictions on the angles $\varphi$ and $\vartheta$. Furthermore, two remarks concerning the implementation should be made:

Firstly, it should be noted that, although we do not evaluate our model $\widetilde{V}$ on $\Omega_R$ but on the ellipsoid $E_{\mathrm{E}}$ which lies in $\Omega_R^{\mathrm{ext}}$ and whose semiminor axis is slightly larger than $R$, this does not reduce the quality and relevance of this study. The 'distance' between $E_{\mathrm{E}}$ and the 'orbit ellipsoid' $E_{\mathrm{S}}$ is still approximately 443 km which was approximately the initial orbit altitude of the satellite in the SST mission CHAMP.

In the implementation, the surfaces $\Omega_R$, $E_{\mathrm{E}}$, and $E_{\mathrm{S}}$ are scaled with the multiplicative factor $0.999/6378136.3$. This scaling maps $\Omega_R$, $E_{\mathrm{E}}$, and $E_{\mathrm{S}}$ on a sphere with radius 0.999, on an ellipsoid of revolution with axes $\widehat{a}_1 = 1$, $\widehat{a}_2 = 1.00336409$, and on an ellipsoid of revolution with axes $\widehat{b}_1 = 1.069097342$, $\widehat{b}_2 = 1.073391987$, respectively. While the values of the potential and the smoothing spline and the errors of this approximation are invariant under the scaling, the matrices in (20) and, consequently, the smoothing parameters are scaled with some multiplicative factor. This means that, apart from the mean absolute error and the rooted mean square error, the data listed in this section refer directly to the implementation for the scaled surfaces.

## 5.2 Local Reconstruction of the Gravitational Potential from Local Noisy SST-Data

The box below lists the data for the numerical simulation:

- A Reuter grid with grid parameter $\tau = 300$ on $\Omega_R$ is projected on $E_S$, and we select those grid points in the local domain $\Gamma_S$ (a domain on $E_S$ over Malaysia), given by

$$\Gamma_S := \left\{ x = (r, \varphi, \vartheta) \in E_S \;\middle|\; \begin{array}{l} \varphi \in [1.396263402, 2.967059728], \\ \vartheta \in [1.047197551, 2.094395102] \end{array} \right\}. \tag{23}$$

  $\Gamma_S$ contains $N = 14306$ points of the projected Reuter grid. (The complete Reuter grid with grid parameter $\tau = 300$ consists of 114444 points.)

- The SST-signal (18) of the potential $\widetilde{V}$ is computed in the $N = 14306$ points in $\Gamma_S$, and noise of a noise level of 2% of the mean absolute value of the SST-signal is added. The (numerically computed) variance of this noise is $\widetilde{\sigma}^2 = 71.1938\ \mathrm{m\,s^{-2}}$.

- Smoothing splines $S_\lambda$ are computed in $\mathcal{H} = \mathcal{H}(\{h^{-n/2}\}; \overline{\Omega_R^{\mathrm{ext}}})$ with $h = 0.93$ from the noisy SST-data (19) for a range of smoothing parameters $\lambda$.

- Due to Gibbs' phenomena at the boundary of the local domain

$$\Gamma_E := \left\{ x = (r, \varphi, \vartheta) \in E_E \;\middle|\; \begin{array}{l} \varphi \in [1.396263402, 2.967059728], \\ \vartheta \in [1.047197551, 2.094395102] \end{array} \right\}, \tag{24}$$

  which is just the projection of $\Gamma_S$ onto $E_E$ along the radial direction, we evaluate the smoothing splines $S_\lambda$ and the potential $\widetilde{V}$ on the subset

$$\widetilde{\Gamma}_E := \left\{ x = (r, \varphi, \vartheta) \in E_E \;\middle|\; \begin{array}{l} \varphi \in [1.625173419, 2.738149711], \\ \vartheta \in [1.199804229, 1.941788424] \end{array} \right\} \tag{25}$$

  on a $(\varphi, \vartheta)$-grid of $140 \times 140$ points, which is equiangular in $\varphi$ and equiangular in $\vartheta$.

- The potential $\widetilde{V}$ assumes on $\widetilde{\Gamma}_E$ values between $-180\ \mathrm{m^2\,s^{-2}}$ and $360\ \mathrm{m^2\,s^{-2}}$.

Table 1 lists the mean absolute error and the rooted mean square error for the computed smoothing splines $S_\lambda = \sum_{i=1}^{N} \alpha_i^\lambda L_i$ with smoothing parameters $\lambda$, that range from $10^{-5}$ to 100. The errors are computed from the values of the splines at the $(\varphi, \vartheta)$-evaluation grid of $140 \times 140$ points on $\widetilde{\Gamma}_E$. The smoothing spline with smoothing parameter $\lambda = 1$ has the smallest mean absolute error and the smallest rooted mean square error.

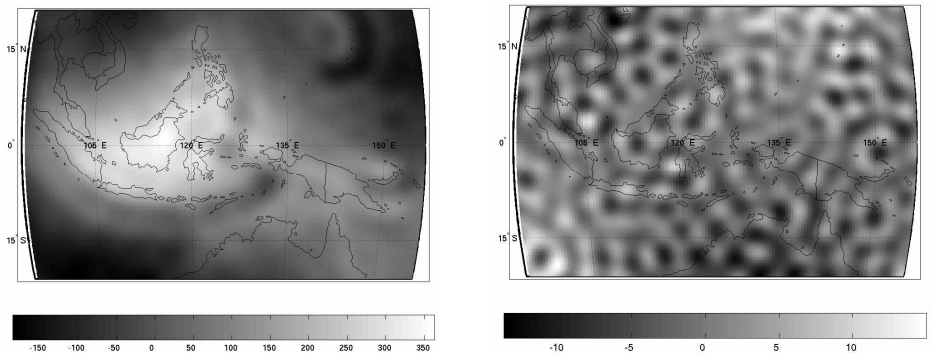


**Figure 7:** *The potential* $\widetilde{V}|_{\widetilde{\Gamma}_E}$ *(left picture) and the error* $(\widetilde{V} - S_\lambda)|_{\widetilde{\Gamma}_E}$ *(right picture) of the smoothing spline* $S_\lambda$, $\lambda = 1$, *in* $\mathrm{m}^2\,\mathrm{s}^{-2}$.

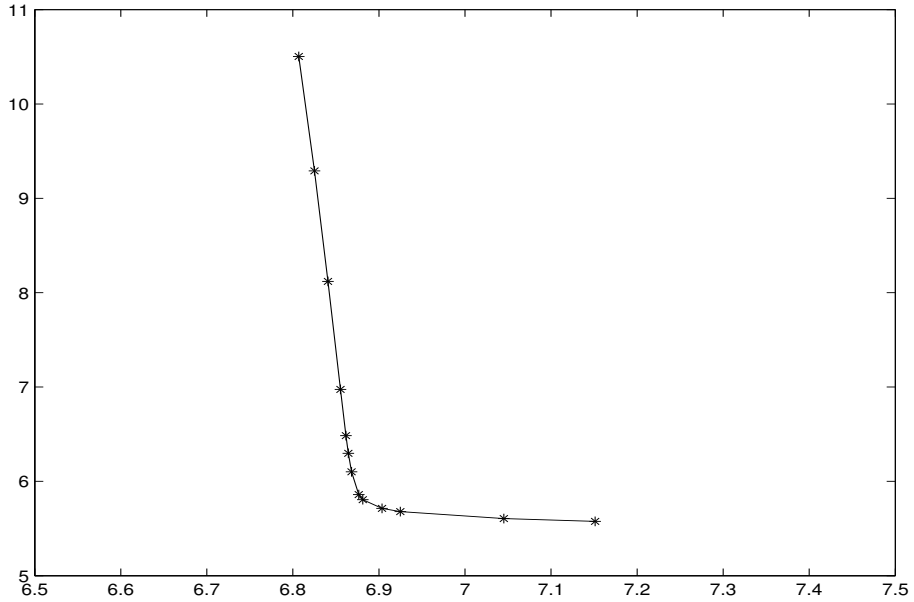


**Figure 8:** *The L-curve* $\lambda \mapsto (\ln(|\mathcal{L}S_\lambda - (\mathcal{L}\widetilde{V} + \epsilon)|), \ln(\|S_\lambda\|_{\mathcal{H}(\{h^{-n/2}\};\overline{\Omega_R^{\mathrm{ext}}})}))$ *for the data given in Table 1, where the smoothing parameters* $\lambda \in \{0.7, 0.85, 2, 3, 4\}$ *are omitted for a better transparency of the plot:* $\ln(|\mathcal{L}S_\lambda - (\mathcal{L}\widetilde{V} + \epsilon)|$ *is plotted on the x-axis and* $\ln(\|S_\lambda\|_{\mathcal{H}(\{h^{-n/2}\};\overline{\Omega_R^{\mathrm{ext}}})})$ *is plotted on the y-axis. The smoothing parameter declines if we follow the L-curve from the right to the left.*

Figure 7 shows the potential $\widetilde{V}|_{\widetilde{\Gamma}_E}$ and the error $(\widetilde{V} - S_\lambda)|_{\widetilde{\Gamma}_E}$ of the smoothing

spline $S_\lambda$ with smoothing parameter $\lambda = 1$.

In order to compare this 'best' smoothing parameter $\lambda = 1$ with the one predicted by the L-curve criterion, Table 1 also lists the quantities $|\mathcal{L}S_\lambda - (\mathcal{L}\widetilde{V} + \epsilon)|$ and $\|S_\lambda\|_{\mathcal{H}(\{h^{-n/2}\};\overline{\Omega_R^{\text{ext}}})}$, where $S_\lambda = \sum_{i=1}^{N} \alpha_i^\lambda L_i$, $\mathcal{L}S_\lambda := (\mathcal{L}_1 S_\lambda, \ldots, \mathcal{L}_N S_\lambda)^T$, $\mathcal{L}\widetilde{V} := (\mathcal{L}_1\widetilde{V}, \ldots, \mathcal{L}_N\widetilde{V})^T$, $\epsilon = (\epsilon_1, \ldots, \epsilon_N)^T$, for various smoothing parameters $\lambda$. Figure 8 shows the *L-curve* for most of the parameters $\lambda$ listed in Table 1. For this scenario the L-curve criterion works satisfactory because the 'corner' of the L-curve corresponds to our experimentally determined 'best' smoothing parameter $\lambda = 1$.

**Table 1:** *The quantities* $|\mathcal{L}S_\lambda - (\mathcal{L}\widetilde{V} + \epsilon)|$, $\|S_\lambda\|_{\mathcal{H}(\{h^{-n/2}\};\overline{\Omega_R^{\text{ext}}})}$, *and the mean absolute error (*mean error*), and the rooted mean square error (*rms error*) of the smoothing splines* $S_\lambda$ *in* $\mathcal{H}(\{h^{-n/2}\};\overline{\Omega_R^{\text{ext}}})$, *where* $h = 0.93$, *with the smoothing parameters* $\lambda$ *(on the* $140 \times 140$ $(\varphi, \vartheta)$*-evaluation grid on* $\widetilde{\Gamma}_{\text{E}}$*).*

| $\lambda$ | $\lvert\mathcal{L}S_\lambda - (\mathcal{L}\widetilde{V} + \epsilon)\rvert$ | $\|S_\lambda\|_{\mathcal{H}(\{h^{-n/2}\};\overline{\Omega_R^{\text{ext}}})}$ | mean error in $\text{m}^2\,\text{s}^{-2}$ | rms error in $\text{m}^2\,\text{s}^{-2}$ |
|---|---|---|---|---|
| $10^{-5}$ | 904.071 | 36470.8 | 115.5329 | 143.347 |
| $10^{-4}$ | 920.715 | 10841.1 | 50.0656 | 62.7500 |
| 0.001 | 935.131 | 3359.14 | 21.4827 | 27.1124 |
| 0.01 | 948.848 | 1069.24 | 9.8564 | 12.2821 |
| 0.03 | 954.991 | 655.133 | 7.0270 | 8.7270 |
| 0.05 | 957.667 | 543.441 | 6.0615 | 7.5408 |
| 0.1 | 961.118 | 446.701 | 5.0041 | 6.2605 |
| 0.5 | 969.261 | 350.697 | 3.3549 | 4.2707 |
| 0.7 | 971.321 | 340.912 | 3.1626 | 4.0318 |
| 0.85 | 972.645 | 335.982 | 3.0868 | 3.9317 |
| 1 | 973.853 | 332.166 | 3.0452 | 3.8718 |
| 2 | 980.494 | 318.124 | 3.0966 | 3.8914 |
| 3 | 986.066 | 311.037 | 3.2869 | 4.1137 |
| 4 | 991.144 | 306.35 | 3.4842 | 4.3540 |
| 5 | 995.917 | 302.874 | 3.6654 | 4.5791 |
| 10 | 1017.31 | 292.778 | 4.3361 | 5.4331 |
| 50 | 1147.21 | 272.153 | 6.1439 | 7.8669 |
| 100 | 1275.66 | 264.074 | 6.9487 | 9.0265 |

In order to illustrate the *Gibbs' phenomena* at the boundary of $\Gamma_{\text{E}}$, we evaluate $S_\lambda$,

with $\lambda = 1$, and $\widetilde{V}$ on a $(\varphi, \vartheta)$-grid of $200 \times 200$ points on $\Gamma_{\mathrm{E}}$ (which is equiangular in $\varphi$ and equiangular in $\vartheta$). After that, we remove cutoff $\in \{0, 10, 20, 30, 40, 50\}$ points in $\varphi$-direction and in $\vartheta$-direction of this grid at the respective sides of the domain $\Gamma_{\mathrm{E}}$ and compute the mean absolute error and the rooted mean square error of $S_\lambda$ as an approximation of $\widetilde{V}$ for the remaining grid points. These errors are listed in Table 2. The evaluation grid of $140 \times 140$ points on our domain $\widetilde{\Gamma}_{\mathrm{E}}$ corresponds to cutoff $= 30$.

**Table 2:** *The mean absolute error (*mean error*) and the rooted mean square error (*rms error*) of the smoothing spline $S_\lambda$ in $\mathcal{H}(\{h^{-n/2}\}; \overline{\Omega_R^{\mathrm{ext}}})$, where $\lambda = 1$, $h = 0.93$, on subdomains of $\Gamma_{\mathrm{E}}$ which are obtained by removing* cutoff *points in $\varphi$-direction and in $\vartheta$-direction of the $200 \times 200$ $(\varphi, \vartheta)$-evaluation grid at the respective sides of the domain $\Gamma_{\mathrm{E}}$.*

| cutoff | mean error in $\mathrm{m}^2\,\mathrm{s}^{-2}$ | rms error in $\mathrm{m}^2\,\mathrm{s}^{-2}$ |
|---|---|---|
| 0 | 5.2649 | 7.3952 |
| 10 | 4.1225 | 5.4831 |
| 20 | 3.4430 | 4.4601 |
| 30 | 3.0452 | 3.8718 |
| 40 | 2.7467 | 3.4540 |
| 50 | 2.6093 | 3.3106 |

Figure 9 shows a multiresolution analysis of the potential $\widetilde{V}|_{\widetilde{\Gamma}_{\mathrm{E}}}$ which has been computed by convolving the 'best' smoothing spline $S_\lambda$ in $\mathcal{H}(\{h^{-n/2}\}; \overline{\Omega_R^{\mathrm{ext}}})$, where $\lambda = 1$, $h = 0.93$, with kernels of the Abel-Poisson scaling function $\{\Phi_j\}_{j \in \mathbb{N}_0}$ for $\mathcal{H}(\{h^{-n/2}\}; \overline{\Omega_R^{\mathrm{ext}}})$ (where $(\Phi_j)\hat{}(n) := e^{-2^{-j}n}$) and of the corresponding wavelet. In formulas, the potential $\widetilde{V}|_{\widetilde{\Gamma}_{\mathrm{E}}}$ is reconstructed by

$$\widetilde{V}|_{\widetilde{\Gamma}_{\mathrm{E}}} \approx P_9 S_\lambda|_{\widetilde{\Gamma}_{\mathrm{E}}} = P_5 S_\lambda|_{\widetilde{\Gamma}_{\mathrm{E}}} + \sum_{j=5}^{8} T_j S_\lambda|_{\widetilde{\Gamma}_{\mathrm{E}}}\,, \tag{26}$$

where $\lambda = 1$, and we have the relation

$$P_{j+1} S_\lambda = P_j S_\lambda + T_j S_\lambda\,.$$

(For the definitions of $P_j S_\lambda$ and $T_j S_\lambda$ see Theorem 3.14 and (21) and (22).)

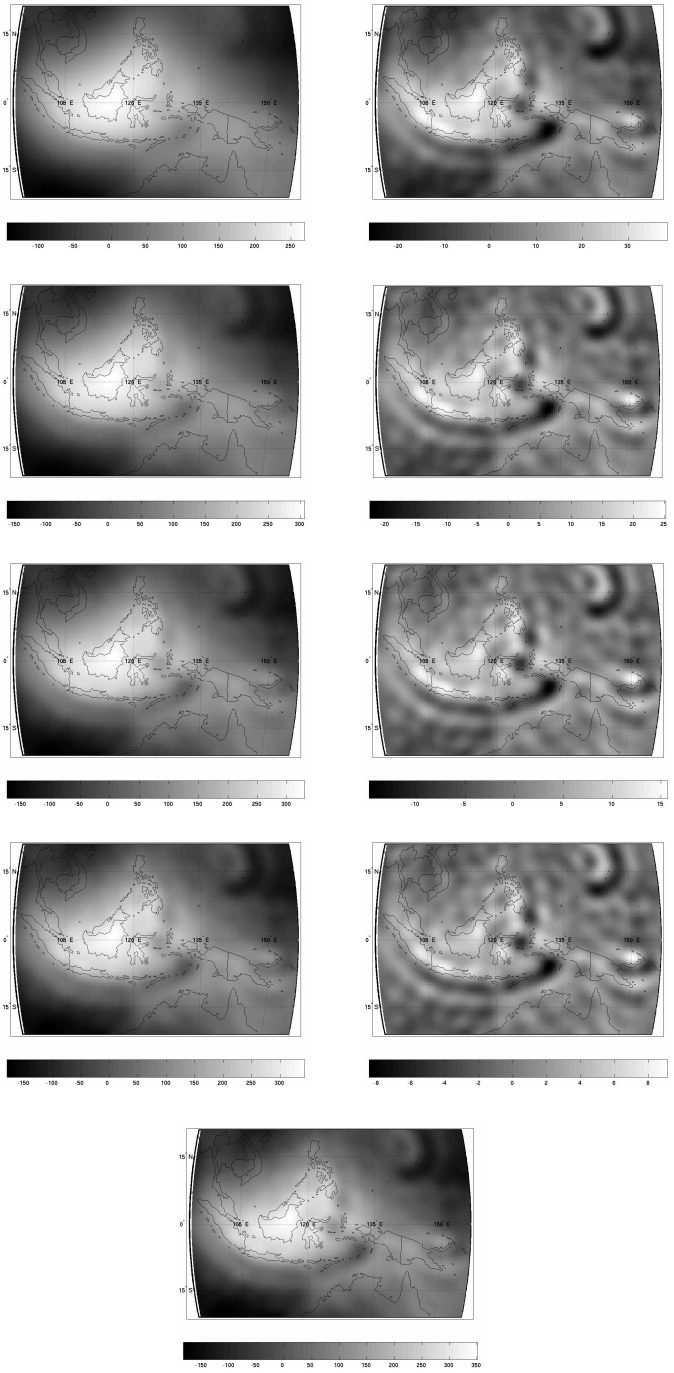

**Figure 9:** *Multiresolution (26) of* $\widetilde{V}|_{\widetilde{\Gamma}_{\mathbf{E}}}$*: in the* $j$*-th row on the left* $P_{j+4}S_\lambda|_{\widetilde{\Gamma}_{\mathbf{E}}}$ *and on the right* $T_{j+4}S_\lambda|_{\widetilde{\Gamma}_{\mathbf{E}}}$*, where* $j \in \{1,2,3,4\}$*, and in the last row* $P_9 S_\lambda|_{\widetilde{\Gamma}_{\mathbf{E}}}$*.*

## 5.3 A Global Model of the Gravitational Potential from Global Noisy SST-Data

The box below lists the data for the numerical simulation:

- Global noisy SST-data of the potential $\widetilde{V}$ is generated in the points on $E_{\mathrm{S}}$, obtained by projecting a Reuter grid with grid parameter $\tau = 150$ along the radial direction from $\Omega_R$ onto $E_{\mathrm{S}}$. The total number of grid points on $E_{\mathrm{S}}$ is $N = 28568$, and the noise has a noise level of 2% of the mean absolute value of the SST-signal. The (numerically computed) variance of this noise is $\widetilde{\sigma} = 61.6225\ \mathrm{m\,s^{-2}}$.
- Smoothing splines $S_\lambda$ in $\mathcal{H}(\{h^{-n/2}\}; \overline{\Omega_R^{\mathrm{ext}}})$, where $h = 0.93$, are computed from this global noisy SST-data for several smoothing parameters $\lambda$ .
- These smoothing splines $S_\lambda$ and the potential $\widetilde{V}$ are evaluated on a global $(\varphi, \vartheta)$-grid which consists of $200 \times 200$ points, equiangular in $\varphi$ and equiangular in $\vartheta$.
- The potential $\widetilde{V}$ assumes on $E_{\mathrm{E}}$ values between $-370\,\mathrm{m^2\,s^{-2}}$ and $+350\,\mathrm{m^2\,s^{-2}}$.

Figure 10 shows the potential $\widetilde{V}$ on the ellipsoid $E_{\mathrm{E}}$ in the left picture and the error $\widetilde{V} - S_\lambda$ of the empirically determined 'best' smoothing spline $S_\lambda$ with $\lambda = 2$ on $E_{\mathrm{E}}$ in the right picture. The mean absolute error of this spline $S_\lambda$ as an approximation of $\widetilde{V}$ on $E_{\mathrm{E}}$ is $3.0763\,\mathrm{m^2\,s^{-2}}$, and its rooted mean square is $3.9472\,\mathrm{m^2\,s^{-2}}$.

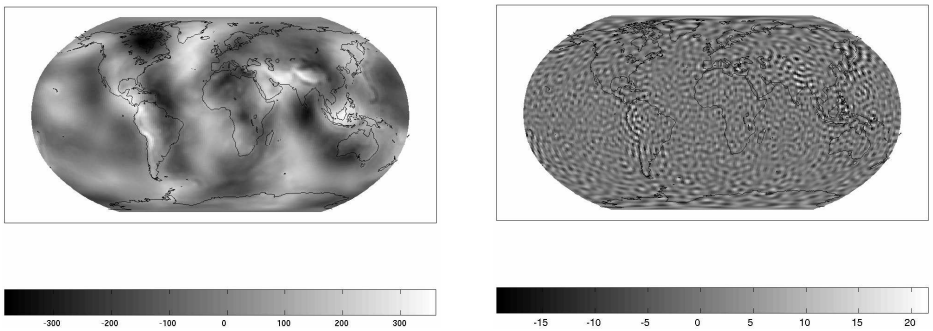


**Figure 10:** *The potential $\widetilde{V}$ on $E_{\mathrm{E}}$ (left picture) and the error $\widetilde{V} - S_\lambda$ of the smoothing spline $S_\lambda$, $\lambda = 2$, on $E_{\mathrm{E}}$ (right picture) in* $\mathrm{m^2 s^{-2}}$.

**Acknowledgment:** The authors acknowledge the financial support of the DFG (Deutsche Forschungsgemeinschaft), Contract No. FR 761/5-1 and FR 761/12-1, and thank the RHRK (Regionales Hochschul-Rechenzentrum Kaiserslautern) for the use of their facilities. Furthermore, we thank M. Fengler for providing his Prama 2001 C++ library.

## References

[1] Antoine, J-P. & Vandergheynst, P. 1999 Wavelets on the 2-sphere and related manifolds. *Rep. Math. Phys.* **43**, 13–24.

[2] Antoine, J-P. & Vandergheynst, P. 1999 Wavelets on the 2-sphere: A group-theoretical approach. *Appl. Comput. Harmon. Anal.* **7**, 262–291.

[3] Aronszajn, N. 1950 Theory of reproducing kernels. *Trans. Amer. Math. Soc.* **68**, 377–404.

[4] Austen, G., Grafarend, E. & Reubelt, T. 2002 Analysis of the Earth's gravitational field from semi-continuous ephemerides of a low Earth orbiting GPS-tracked satellite of type CHAMP, GRACE, or GOCE. *Vistas for Geodesy in the New Millenium* (J. Adam and K.P. Schwarz, eds.). Berlin, Heidelberg: Springer Verlag, 309–315.

[5] Backus, G., Parker, R. & Constable, C. 1996 *Foundations of Geomagnetism.* Cambridge University Press.

[6] Baumann, P. 2001 *Regularization of Inverse Problems in Satellite Geodesy by Wavelet Methods with Orbital Data Given on Closed Surfaces.* Diploma Thesis, Geomathematics Group, Laboratory of Technomathematics, University of Kaiserslautern.

[7] Beatson, R. K., Light, W. A. & Billings, S. 2000 Fast solution of the radial basis function interpolation equations: Domain decomposition methods. *SIAM J. Sci. Comput.* **22**, 1717–1740.

[8] Engl, H. W., Hanke, M. & Neubauer, A. 1996 *Regularization of Inverse Problems.* Dordrecht: Kluwer Academic Publishers.

[9] ESA 1996 *The Nine Candidate Earth Explorer Missions.* Nordwijk: Publications Division ESTEC, SP-1196 (1).

[10] ESA 1998 *European Views on Dedicated Gravity Field Missions: GRACE and GOCE.* An Earth Sciences Division Consultation Document, ESD-MAG-REP-CON-001, European Space Agency.

[11] ESA 1999 *Gravity Field and Steady-State Ocean Circulation Mission.* Noordwijk: ESTEC, ESA SP-1233 (1).

[12] Freeden, W. 1980 On the approximation of the external gravitational potential with closed systems of (trial) functions. *Bull. Géod.* **54**, 1–20.

[13] Freeden, W. 1981 On spherical spline interpolation and approximation. *Math. Meth. Appl. Sci.* **3**, 551–575.

[14] Freeden, W. 1981 On approximation by harmonic splines. *Manuscr. Geod.* **6**, 193–244.

[15] Freeden, W. 1982 Interpolation and best approximation by harmonic spline functions. *Boll. Geod. Sci. Aff.* **1**, 105–120.

[16] Freeden, W. 1982 On spline methods in geodetic approximation problems. *Math. Meth. Appl. Sci.* **4**, 382–396.

[17] Freeden, W. 1999 *Multicsale Modelling of Spaceborne Geodata.* Stuttgart, Leipzig: B. G. Teubner.

[18] Freeden, W., Gervens, T. & Schreiner, M. 1998 *Constructive Approximation on the Sphere (With Applications to Geomathematics).* Oxford: Oxford Science Publications, Clarendon Press.

[19] Freeden, W., Glockner, O. & Thalhammer, M. 1999 Multiscale gravitational field recovery from GPS-satellite-to-satellite tracking. *Studia Geophys. et Geod.* **43**, 229–264.

[20] Freeden, W. & Hesse, K. 2002 Spline modelling of geostrophic flow: Theoretical and numerical aspects. *Reports of the Technomathematics Group No. 250*, University of Kaiserslautern (submitted to *Numerische Mathematik*).

[21] Glockner, O. 2002 *On Numerical Aspects of Gravitational Field Modelling from SST and SGG by Harmonic Splines and Wavelets (With Application to CHAMP Data).* Doctoral Thesis, Geomathematics Group, Department of Mathematics, University of Kaiserslautern, Aachen: Shaker Verlag.

[22] Göttelmann, J. 1996 Locally supported wavelets on the sphere. *Preprint, No. 14*, Dept. of Math., University of Mainz.

[23] Griebel, M. & Oswald, P. 1995 On the abstract theory of additive and multiplicative Schwarz algorithms. *Numer. Math.* **70**, 163–180.

[24] Gutting, M. 2002 *Multiscale Gravitational Field Modeling from Oblique Derivatives.* Diploma Thesis, Geomathematics Group, Department of Mathematics, University of Kaiserslautern.

[25] Hesse, K. 2003 *Domain Decomposition Methods in Multiscale Geopotential Determination from SST and SGG.* Doctoral Thesis, Geomathematics Group, Department of Mathematics, University of Kaiserslautern, Aachen: Shaker Verlag.

[26] Holschneider, M. 1996 Continuous wavelet transforms on the sphere. *J. Math. Phys.* **37**, 4156–4165.

[27] Kirsch, A. 1996 *An Introduction to the Mathematical Theory of Inverse Problems.* New York: Springer-Verlag.

[28] Lemoine, F. G., Kenyon, S. C., Factor, J. K., Trimmer, R. G., Pavlis, N. K., Chinn, D. S., Cox, C. M., Klosko, S. M., Luthcke, S. B., Torrence, M. H., Wang, Y. M., Williamson, R. G., Pavlis, E. C., Rapp, R. H. & Olson, T. R. 1998 *The Development of the Joint NASA GSFC and NIMA Geopotential Model EGM96.* NASA/TP–1998–206861.

[29] Lions, P. L. 1988 On the Schwarz alternating method I. *Proceedings of the 1st International Symposium on Domain Decomposition Methods for Partial Differential Equations*, Paris, January 1987 (R. Glowinski, G. H. Golub, G. A. Meurant, and J. Periaux, eds.). Philadelphia: SIAM, pp. 1–42.

[30] P. L. Lions. 1999 On the Schwarz alternating method II: Stochastic interpretation and order properties. *Proceedings of the 2nd International Symposium on Domain Decomposition Methods*, Los Angeles, California, January 1988 (T. Chan, R. Glowinski, J. Periaux, and O. B. Widlund, eds.). Philadelphia: SIAM, 47–70.

[31] Müller, C. 1966 *Spherical Harmonics.* Lecture Notes in Mathematics **17**, Berlin, Heidelberg, New York: Springer-Verlag.

[32] Nutz, H. 2002 *A Unified Setup of Gravitational Field Observables.* Doctoral Thesis, Geomathematics Group, Department of Mathematics, University of Kaiserslautern, Aachen: Shaker Verlag.

[33] Schäfer, C. 2001 Space gravity spectroscopy – the sensitvity analysis of GPS-tracked satellite missions (case study CHAMP). Deutsche Geodätische Kommission, Bayerische Akademie der Wissenschaften, *Report C 534*, München.

[34] Sweldens, W. 1995 The lifting scheme: A new philosophy in biorthogonal wavelet constructions. *Wavelet Applications in Signal and Image Processing III* (A. F. Laine, M. A. Unser eds.), SPIE 2569, 68–79.

[35] Sweldens, W. 1997 The lifting scheme: A construction of second generation wavelets. *SIAM J. Math. Anal.* **29**, 511-546.

[36] Vandergheynst, P. 1998 *Ondolettes Directionnelles et Ondolettes sur la Sphère.* Thèse de Doctorat, Univ. Cath. Louvain, Louvain-la-Neuve.

[37] Wahba, G. 1990 *Spline Models for Observational Data.* CBMS-NSF Regional Conference Series in Applied Mathematics, **59**, Philadelphia: SIAM.

[38] Xu, J. 1992 Iterative methods by space decomposition and subspace correction. *SIAM Rev.* **34**, 581–613.

[39] Yamabe, H. 1950 On an extension of the Helly's theorem. *Osaka Mathematical Journal* **2**, 15–17.